Improvement on Hydrogen Storage Property of Ammonia Borane System and Aluminum Hydride System

Graduate School of Engineering
Division of Materials Science and Engineering
Laboratory of Advanced Materials
Chung Hyun LEE

CONTENTS

Chapter 1 General introduction

1.1 Hydrogen energy

Hydrogen is one of the most abundant elements in the universe. It has been estimated that hydrogen makes up more than 90% of all the atoms or 75% of the mass of the universe. And hydrogen has high energy density, and can be made by the electrolysis of water.[1] Furthermore, hydrogen is regenerative and environmentally friendly. Considering the increasing pollution and depletion of fossil energy resources, new energy concepts such as hydrogen are essential for the future of society. Hydrogen does not produce carbon dioxide upon combustion, which as a greenhouse gas is largely responsible for global warming. The ideal hydrogen energy cycle is shown in Fig. 1.

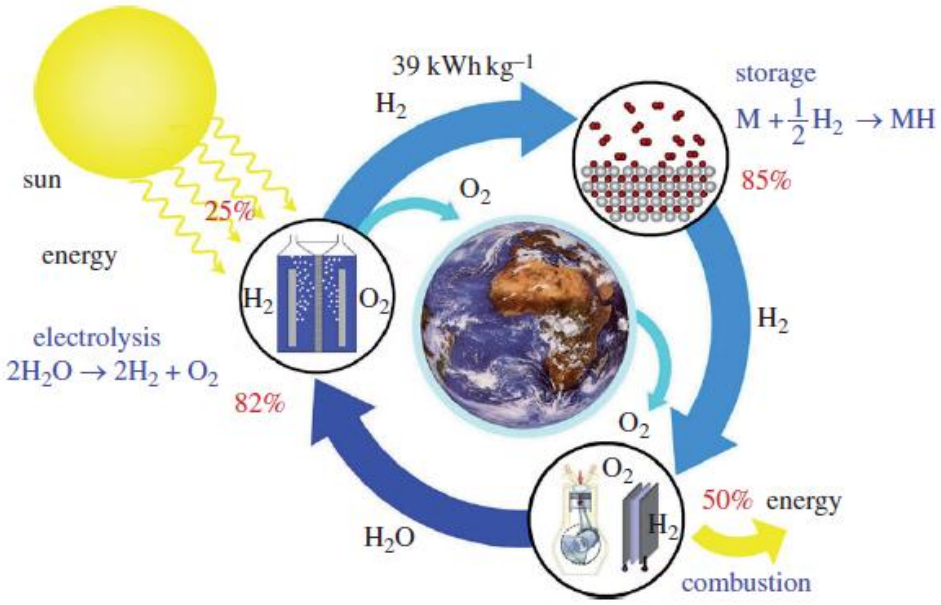

Fig. 1 Ideal hydrogen energy cycle [2]

The hydrogen energy cycle is similar to natural carbon cycle. In this cycle, hydrogen is made by electrolysis of water. Electricity is supplied from a renewable energy source such as solar energy or geothermal energy. Hydrogen as a gas occupies a large volume ($11m^3/kg$) under ambient conditions. So, hydrogen is stored in solid metal hydride to reduce the volume of gas. To produce energy, hydrogen is reacted with oxygen in the fuel cell.[2] However, there are some kinds of problems in realizing this cycle. It is the production, transport and storage of hydrogen. Although hydrogen is the most abundant

element on earth, it has to be produced. There are several methods for producing hydrogen, a method which is widely used at present is using fossil fuels by means of the reaction $-CH_2^- + 2H_2O \rightarrow 3H_2 + CO_2$ at an elevated temperatures (>850 ℃). [3] However, hydrogen production of fossil fuels produces the same amount of carbon dioxide as the direct burning of the fossil fuel. Direct pyrolysis of H_2O requires temperatures above 2,000 ^oC (900 ^oC with a catalyst) [4]. Hydrogen is a renewable fuel, but only if hydrogen is produced directly from solar energy by photovoltaic cells or indirectly though electricity from a renewable source (for example: wind-power or hydro-power) [3]. Figure 2 shows the primary energy sources considered and their routes to hydrogen [5]. Hydrogen produced from energy resources in red square is free of carbon dioxide. However, most power plants are built in specific areas and hydrogen storage is required to transport hydrogen from power plant to the actual location of use. Therefore, for the hydrogen society, we need a way to store hydrogen more compact and lighter.

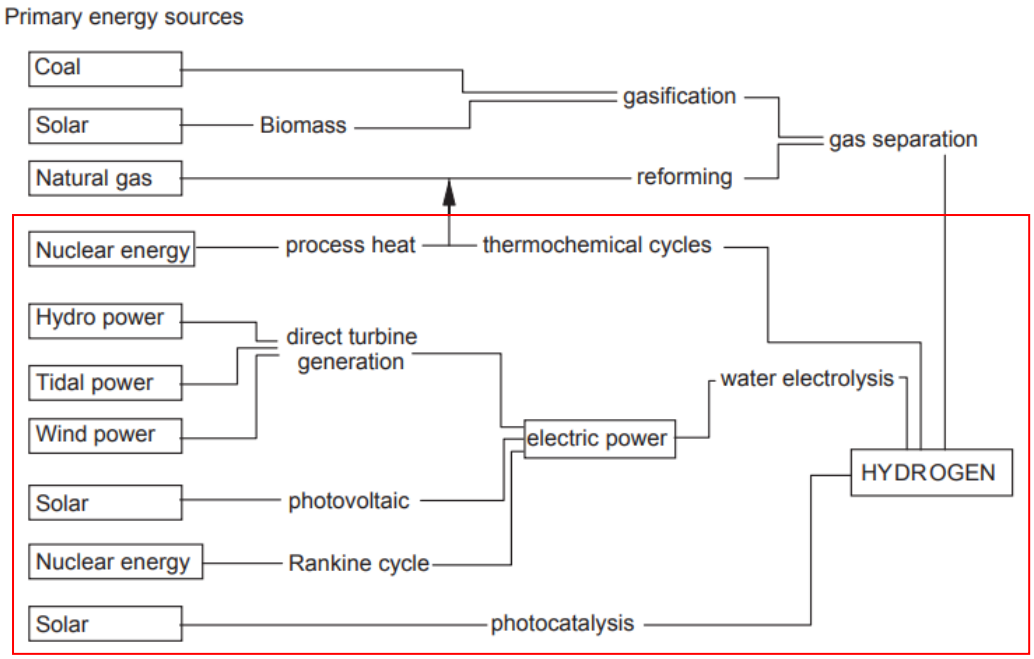

Fig. 2 The primary energy sources considered and their routes to hydrogen [5].

1.2 Hydrogen storage

Hydrogen has an excellent energy density per unit mass, however is has a low volume density. Thus, hydrogen storage at a reasonable energy density is a technical

and economic challenge. Generally, hydrogen is stored in pure form using compression or liquefaction methods. A new approach based on physical or chemical storage materials has been widely recognized and studied over the last few decades.

1.2.1 Compressed hydrogen

Compressed gas is the most used technology for all kinds of gas storage. The gas is generally compressed to a pressure of 200 to 350 bar. More recently, storage pressures above 700 bar are using carbon fiber-reinforced tanks. The system gravimetric capacity of 700 bar compressed hydrogen tank is 4.2 mass% [6]. The design of such a container is detailed in Fig. 3 [7]. TOYOTA, HYUNDAI and HONDA have recently started selling fuel cell vehicles. However, there are still some disadvantages. One is the risk of hydrogen leaks or spills. The tank contains high pressure hydrogen. Once hydrogen is released into the environment, it will result in a hazardous situation. In addition, the gravimetric and volumetric of hydrogen are not sufficiently high.

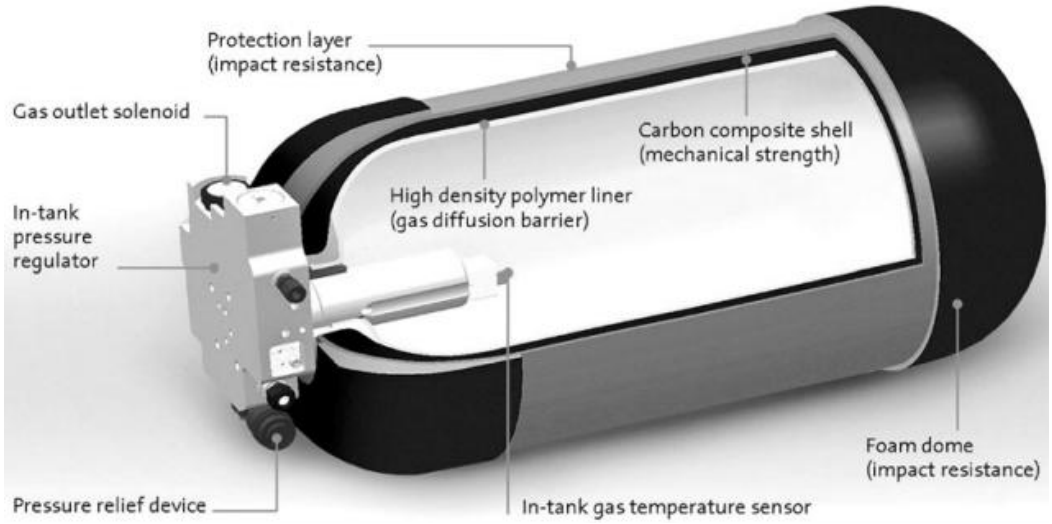

Fig. 3 Type IV compressed gaseous hydrogen vessel [7].

1.2.2 Liquid hydrogen

Hydrogen should be cooled to 20.28 K (-252.87 °C) to be present as a liquid. Liquefaction increases the density to 80 kg/m^3 at 22 K and a pressure of 4 bar, however causes another challenge [8]. First of all, low operating temperatures of 20 to 30 K require a sophisticated cryogenic system and consume a large amount of energy. Second,

heat leakage is inevitable because of the huge difference in temperature from atmosphere (300 K). Therefore, hydrogen evaporates in the vessel and increases the internal pressure. So, liquid hydrogen containers should be fitted with suitable pressure relief systems and safety valves. Evaporation losses on tank unit are 0.3 % to 3 % per day.

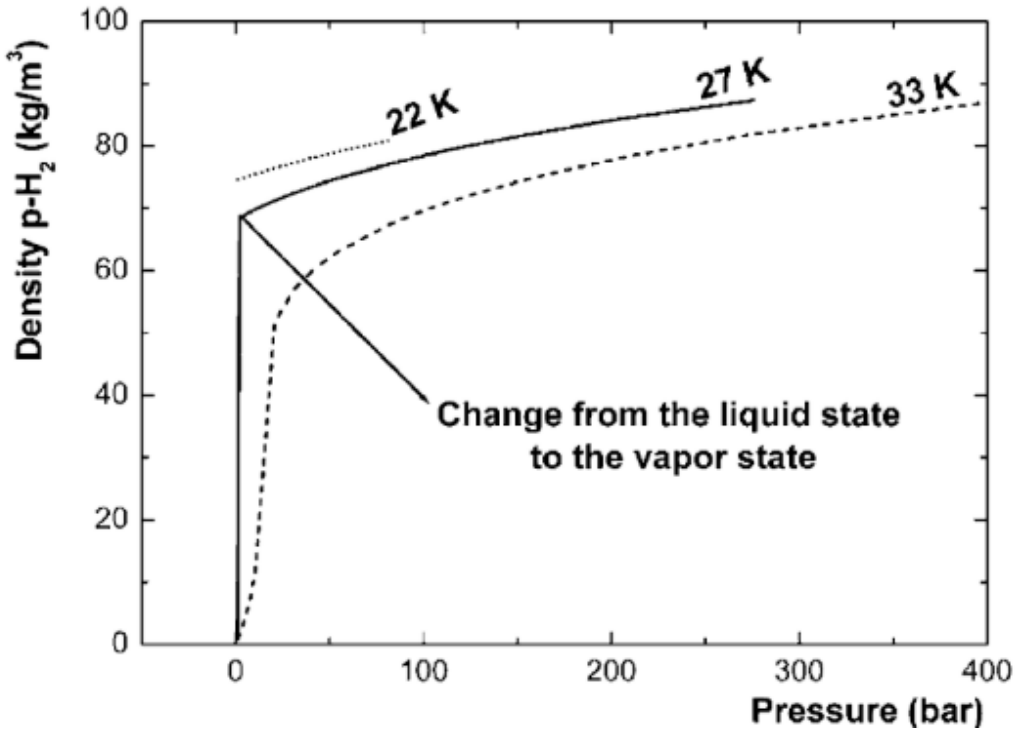

Fig. 4 Evolution of the density of liquid hydrogen as a function of pressure at three different temperatures [8]

1.2.3 Chemical hydrogen storage

Hydrogen could be stored in a compound, where hydrogen binds with other elements chemically. If necessary, the compounds can be decomposed at 100 - 300 °C under specific conditions, typically in vacuum, to regenerate the hydrogen gas. Therefore, this kind of compound can be used reversibly as a hydrogen storage medium. And chemical hydrogen storage can store hydrogen in a compact package compared to compressed hydrogen gas tank and liquid hydrogen. Good storage medium requires properties such as high hydrogen capacity, absorption and release at moderate temperatures and

pressure, low cost and abundant resource, easy handling [9]. According to the US Department of Energy (DOE) target for on-board hydrogen storage systems for light-weight vehicles, a gravimetric and volumetric density were 5.5 mass% and 40 g/L in 2017, respectively [10]. The Japan New Energy and Industrial Technolofy Development Organization (NEDO) also set the technical target [11]. Targets until 2020 were 6.0 mass% and 50 g/L and those until 2030 7.5 mass% and 70g/L. Since these values include the weight and volume of the tank, the value of material-basis should be much larger than those of system-basis. Figure 5 shows the plot of hydrogen storage materials as a function of observed temperature release or sorption. Although various hydrogen storage materials exist, in this paper, only metal hydrides, complex hydrides, amides and imides, ammonia borane are used as examples.

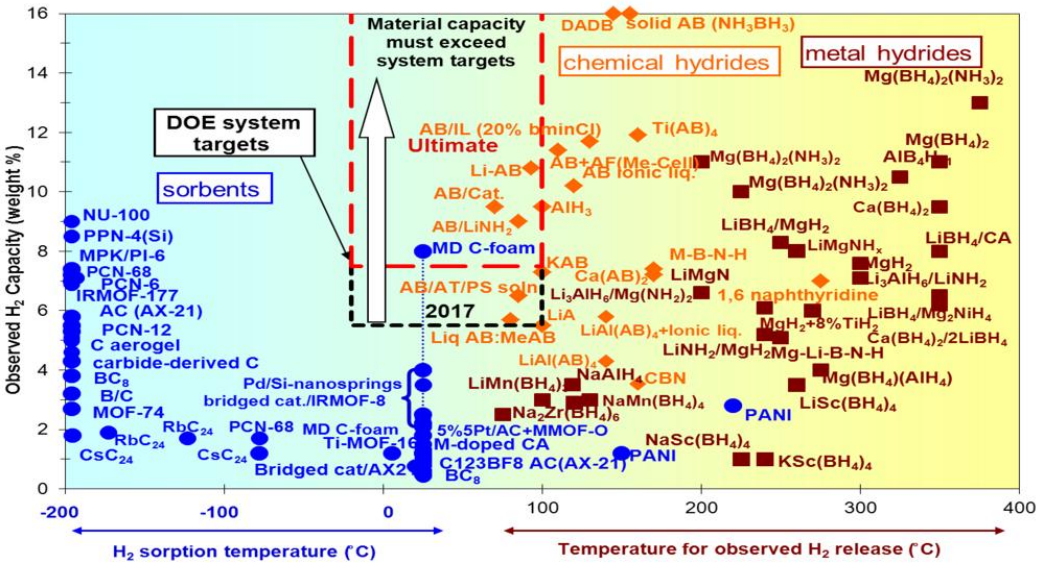

Fig. 5 Plot of hydrogen storage materials as a function of observed temperature release or sorption. (dashed lines denotes DOE 2017 and ultimate targets) [12].

1.3 Hydrogen storage materials

1.3.1 Metal hydrides

Metal hydrides, which can be defined as single phase compounds enriched between the metal and hydrogen, are promising candidates in the field of hydrogen storage [13].

Hydrides exist as ionic, covalent and metallic hydrides. Figure 6 shows the table of the binary hydrides. Hydrogen reacts with many metals and their alloys at elevated temperatures to form hydrides. The lattice structure is a typical metal structure with hydrogen atoms in the gaps. For this reason they are called interstitial hydrides. This type of structure has the limiting compositions MH, MH_2 and MH_3. The hydrogen carries a partial negative charge, depending on the metal [14, 15]. In the alkali metal and alkaline earth metal hydrides, hydrogen exists as a negatively charged ion [16, 17]. These hydrides are called ionic hydrides (e.g. LiH, NaH, CaH_2 etc.). The ionic hydrides are too stable for hydrogen storage. For example, LiH does not decomposed at temperatures below 600 °C. In the covalent hydrides, hydrogen retains covalent bonds with metals. Typical covalent hydride is aluminum hydride, which are large gravimetric and volumetric capacity (10.1 mass%, 149 kg/m^3 respectively). In addition, it releases hydrogen at a low temperature of around 150 °C. However re-hydrogenation of aluminum requires over 100 MPa of hydrogen pressure at room temperature [18]. In the metallic hydrides, hydrogen occupies the interstitial sites between metal atoms. The metals are usually transition metals. Further, the intermetallic compounds can be designed with hydrogen storage properties by mixing metals with different hydrogen storage properties. Table 1 shows the well known intermetallic compounds, such as $LaNi_5$ and TiFe [3]. These materials can reversibly absorb hydrogen at low temperature. However, hydrogen capacity is below 3 wt% because these metals are heavy.

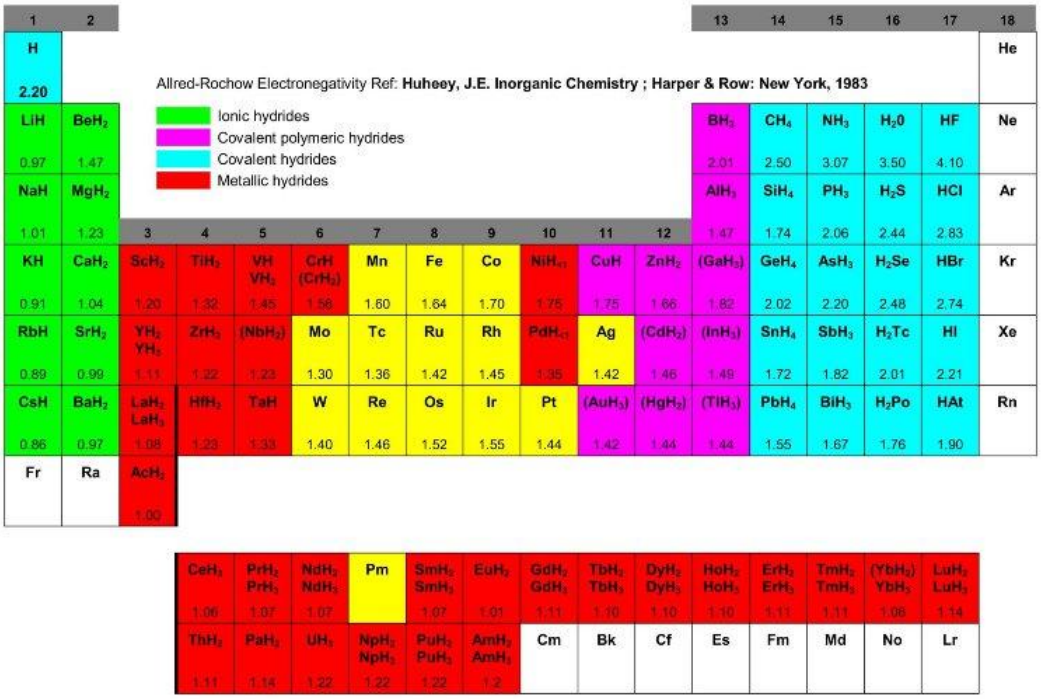

Fig. 6 Table of the binary hydrides and the Allred-Rochow electronegativity. Most elements react with hydrogen to form ionic, covalent or metallic binary hydrides [18].

Table 1 The most important families of hydride forming intermetallic compounds [3].

Intermetallic compound	Prototype	Hydrides	Structure
AB_5	$LaNi_5$	$LaNiH_6$	Haucke phases, hexagonal
AB_2	ZrV_2, $ZrMn_2$, $TiMn_2$	$ZrV_2H_{5.5}$	Laves phase, hexagonal or cubic
AB_3	$CeNi_3$, YFe_3	$CeNi_3H_4$	Hexagonal, $PuNi_3$-type
A_2B_7	Y_2Ni_7, Th_2Fe_7	$Y_2Ni_7H_3$	Hexagonal, Ce_2Ni_7-type
A_6B_{23}	Y_6Fe_{23}	$Ho_6Fe_{23}H_{12}$	Cubic, Th_6Mn_{23}-type
AB	TiFe, ZrNi	$TiFeH_2$	Cubic, CsCl- or CrB-type
A_2B	Mg_2Ni, Ti_2Ni	Mg_2NiH_4	Cubic, $MoSi_2$- or Ti_2Ni-type

1.3.2 Complex hydrides (Alanate and Borohydride)

Complex hydrides are substances such as salts in which hydrogen is covalently bonded to a central atom. Alanate has a light weight and a large number of hydrogen atoms stored per metal atom [19]. In the case of $NaAlH_4$, which is renowned for alanate, the use of Ti as catalyst improves the hydrogen absorption and desorption properties of $NaAlH_4$ [20]. Alkali metal alanates undergo dehydrogenation in the 200-300 ℃ temperature range (Li: 200 °C [21], Na: 210 °C [20], K: 300 °C [22]) to give aluminum metal and the corresponding alkali metal hydrides (1-1).

$$3NaAlH_4 \rightarrow Na_3AlH_6 + 2Al + 3H_2 \qquad (1\text{-}1)$$

Additional removal of hydrogen to produce aluminum and NaH occurrs through a separate reaction (1-2) at 250 °C.

$$Na_3AlH_6 \rightarrow 3NaH + Al + 3/2H_2 \qquad (1\text{-}2)$$

Borohydrides are usually formed from alkali or alkaline earth metals and $[BH_4]^-$ anion. As a representative complex borohydride, LiBH4 with a hydrogen capacity of 18.4 mass% was studied by Schlesinger in 1939 [23]. The decomposition reaction of $LiBH_4$ was described in three steps [24]. First, a structure change accompanied with 0.3 mass% of hydrogen release occurred at 108 °C. The first major hydrogen release occurred at 320 °C releasing 1 mass% of hydrogen (reaction 1-3). A second hydrogen release took place from 400 °C to 600 °C, giving a total amount of 9 wt% (reaction1-4).

$$LiBH_4 \rightarrow LiBH_2 + H_2 \qquad (1\text{-}3)$$

$$LiBH_2 \rightarrow LiH + B + 1/2\ H_2 \qquad (1\text{-}4)$$

Alkaline earth and transition metal borohydrides ($Mg(BH_4)_2$ [25], $Ca(BH_4)_2$ [26], $Zn(BH_4)_2$ [27]) have been also reported.

1.3.3 Ammonia Borane

Ammonia borane (NH_3BH_3, AB), which has a high hydrogen storage capacity of 19.4 wt.% and a volume density of 160 gH_2L^{-1}, is one of the most promising hydrogen storage materials. It can release hydrogen at relatively low temperature range [28]. The molecular structure of AB is similar to ethane (C_2H_6). AB is non-flammable and non-explosive under standard condition, it decomposed in two stages under low temperature range of 70 - 200 °C, to release 6.5 mass% of hydrogen at each step [29]. The solid state AB represents a shorter BH - HN molecular distance than the *van der Waals* distance [30].

On the other hand, NH_3BH_3 has three problems to be realized as a hydrogen storage material. One is the AB has complicated decomposition reaction. AB doesn`t include any metals as constituent atoms. So, dehydrogenation mechanism of AB is difficult from the metal hydrides. Figure 7 shows one of several decomposition reaction of AB. AB thermally decomposed between 70 °C - 112 °C into polyaminoborane, $[NH_2BH_2]_n$, and hydrogen as shown in reaction (1-5). The second step occurs in the range of 110 °C

– 200 °C with further hydrogen loss, forming polyiminoborane, $[NHBH]_n$, and a small fraction of borazine, $[N3_{B3}H_6]$, reactions (1-6) and (1.7) respectively. The decomposition of $[NHBH]_n$ to BN occurs at temperatures of 500 °C - 600 °C, reaction (1-8) [31].

$$n\ NH_3BH_3\ (s) \rightarrow [NH_2BH_2]_n\ (s) + n\ H_2 \qquad (1\text{-}5)$$

$$[NH_2BH_2]_n\ (s) \rightarrow [NHBH]_n\ (s) + n\ H_2 \qquad (1\text{-}6)$$

$$[NH_2BH_2]_n\ (s) \rightarrow [N_3B_3H_6]_{n/3}\ (l) + n\ H_2 \qquad (1\text{-}7)$$

$$[NHBH]_n \rightarrow n\ BN + n\ H_2 \qquad (1\text{-}8)$$

Second is the reversibility for hydrogen desorption and absorption. AB desorbs hydrogen in exothermic reactions in the first and second steps (reaction 1-5, 1-6, 1-7). Only the 3rd step (reaction 1-8) desorbs hydrogen in an endothermic reaction. Therefore, re-hydrogenation of decomposed AB is thermodynamically difficult.

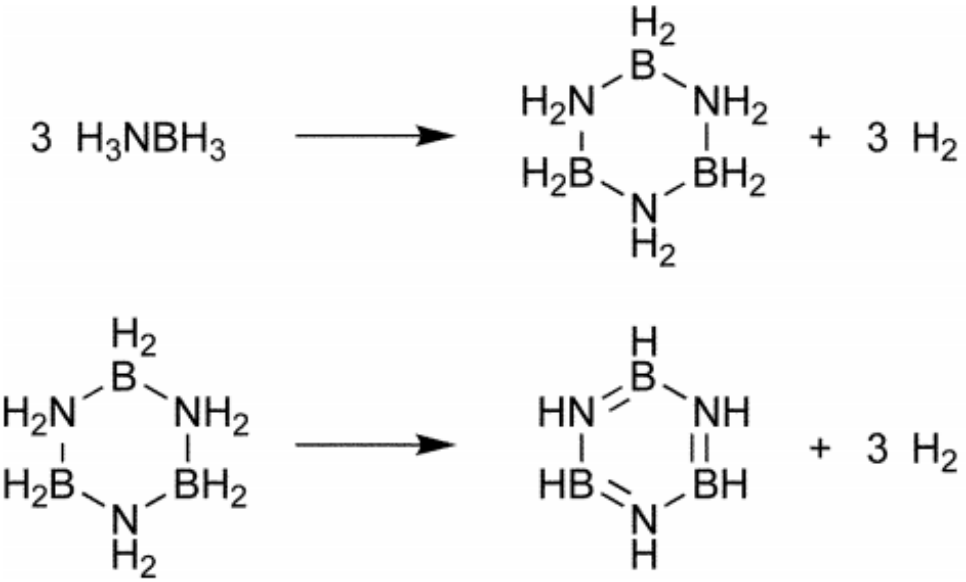

Fig. 7 Dehydrogenation of ammonia borane to from cyclic species polyaminoborane and polyiminoborane [28].

The other is the emission of by-product gases, such as ammonia and borazine, which make significant damage on fuel cells. These gases are generated in a complicated decomposition process of NH_3BH_3. [32] Figure 8 shows the types of gas emission of AB in decomposition reaction. monomeric aminoborane and borazine were identified in the

vapors. The formation of BH_2NH_2 and $(BHNH)_3$ was confirmed in all decomposition steps.

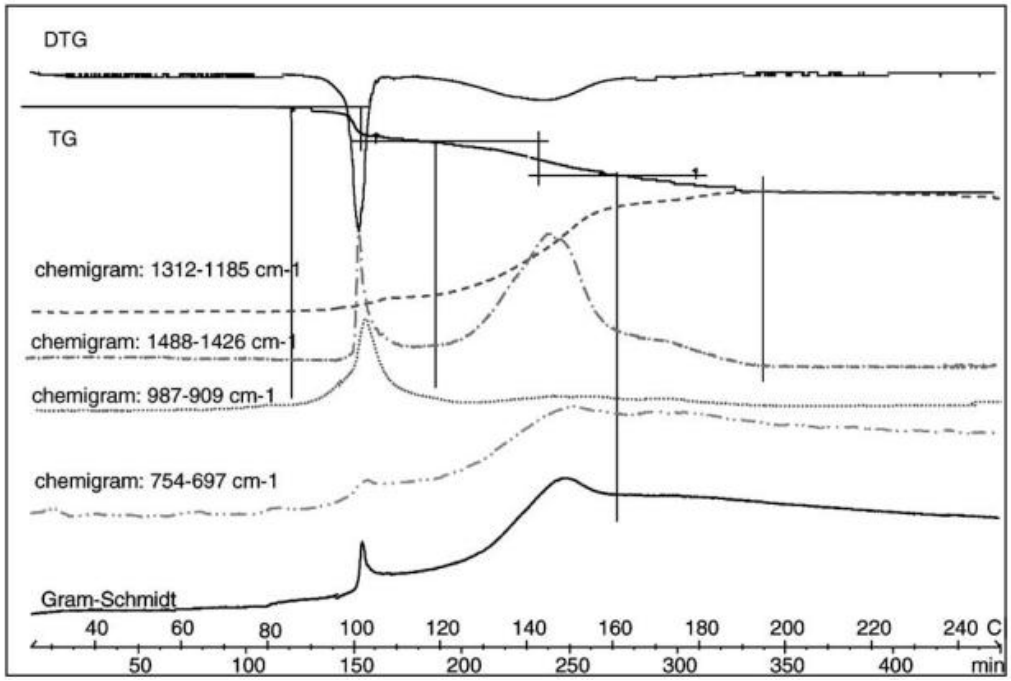

Fig. 8 Simultaneous TG/FTIR analysis of the released gas phase during the thermal decomposition of AB : mass loss, chemigram monomeric aminoborane, chmigram borazine, Gram-Schmidt curve [32].

In order to solve these problems, many studies have been conducted. The catalyst was added to suppress the by-product gas and/or lower the decomposition temperature [33-35]. Also, the researches aiming at the improvement of sorption properties have been done by synthesizing metal amidoborane [36-41]. Its significance lies in the chemical modification of AB by replacing one of H atoms with an alkali or alkaline earth metal to form metal amidoborane. The formation reaction of metal amidoborane is described using AB and metal hydride (MH) as below (reaction 1-9).

$$MH_n + n\ NH_3BH_3 \rightarrow M(NH_2BH_3)_n + n\ H_2\ (M = Li, Na, K, Mg, Ca, Al\ etc.) \quad (1\text{-}9)$$

Metal amidoborane can be synthesized by solid phase method (e.g. ball-milling) or liquid phase method (e.g. the reaction between AB and sodium amide in THF (tetrahydrofuran) [43]). The method of synthesis is different depending on which metal hydride is used. KNH_2BH_3 was synthesized by liquid phase method, whereas solid phase method was not possible [44]. On the other hands, $NaNH_2BH_3$ can be synthesized

by liquid phase [45] and solid phase [42]. In this way, the synthesis method is different according to metal species. The outstanding properties of metal amidobarne are its decomposition temperature and in suppressing the by-products gas emissions. Figure 9 shows the hydrogen and borazine mass spectra of AB, $LiNH_2BH_3$, $NaNH_2BH_3$ samples. In the MS results for hydrogen, AB has 2 steps of hydrogen emission peaks, while $LiNH_2BH_3$ and $NaNH_2BH_3$ have a single emission peak at a lower temperature. And $LiNH_2BH_3$ and $NaNH_2BH_3$ do not confirm release of borazine.

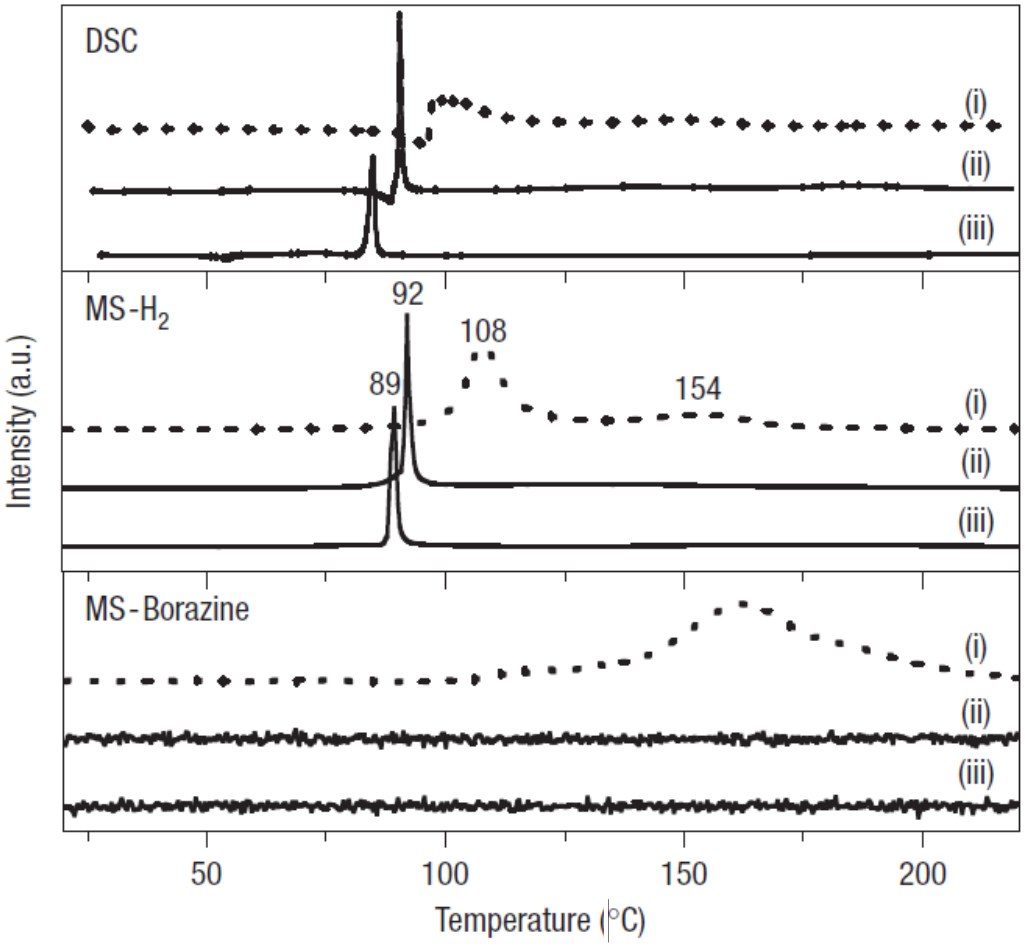

Fig. 9 DSC and MS profiles of (i) AB, (ii) $LiNH_2BH_3$, (iii) $NaNH_2BH_3$ [31]

Despite these advantages, metal amidoborane could not improve the irreversibility which is the biggest disadvantage of AB.

Recently, dual-metal amidoborane has been studied in various directions [41, 46-51]. Among them, $LiNa(NH_2BH_3)_2$ was the first dual-metal amidoborane to be discovered. Figure10 shows the TG-DSC-MS profiles of $LiNa(NH_2BH_3)_2$ [46]. Considering only the

hydrogen release properties, LiNa(NH2BH3)2 has changed to be poorer. Not only hydrogen but also ammonia and NH_2BH_3 were released.

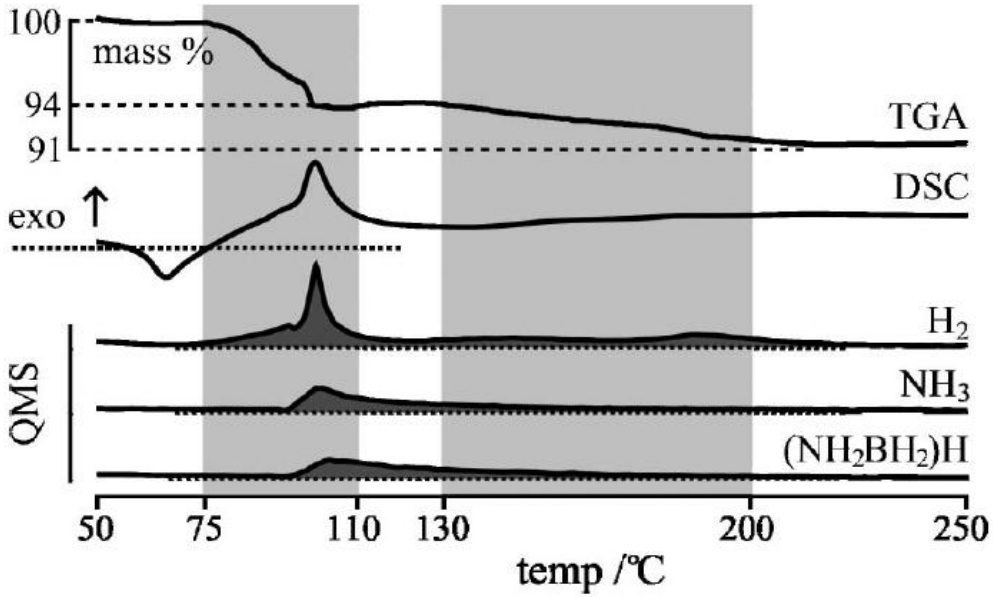

Fig. 10 TG-DSC-MS profiles of $LiNa(NH_2BH_3)_2$ [46]

Meanwhile, Na-Mg amidoborane, which is a thermodynamically stable material and is expected to occur with endothermic decomposition reaction, was found [47-49]. In the previous studies, endothermic hydrogen release reactions were reported in two kinds of Na-Mg amidoboranes, $NaMg(NH_2BH_3)_3$ [49] and $Na_2Mg(NH_2BH_3)_4$ [47, 48]. In the case of $Na_2Mg(NH_2BH_3)_4$, two synthesis methods were used. One is to mix AB, MgH_2 in certain molar ratio and synthesize them by ball-milling under 1 bar He at 200 rpm for 80 min [47]. The other is to mix $Mg(NH_2BH_3)_2 \cdot NH_3$ and NaH in the molar ratio of 1 : 1 and milled at 200 rpm for 10 hours. Figure 11 and 12 show the TG/DSC/MS profiles of $NaMg(NH_2BH_3)_3$ [49] and $Na_2Mg(NH_2BH_3)_4$ [48] respectively. Both samples have endothermic hydrogen release reaction at temperature around 170 °C. However, there is a notable difference between hydrogen emission reactions. In case of $NaMg(NH_2BH_3)_3$, it has a complex 4 step hydrogen release reaction. On the other hand, $Na_2Mg(NH_2BH_3)_4$ has only single endothermic dehydrogenation reaction. This suggests that the sample of $NaMg(NH_2BH_3)_3$ is likely to contain other impurities.

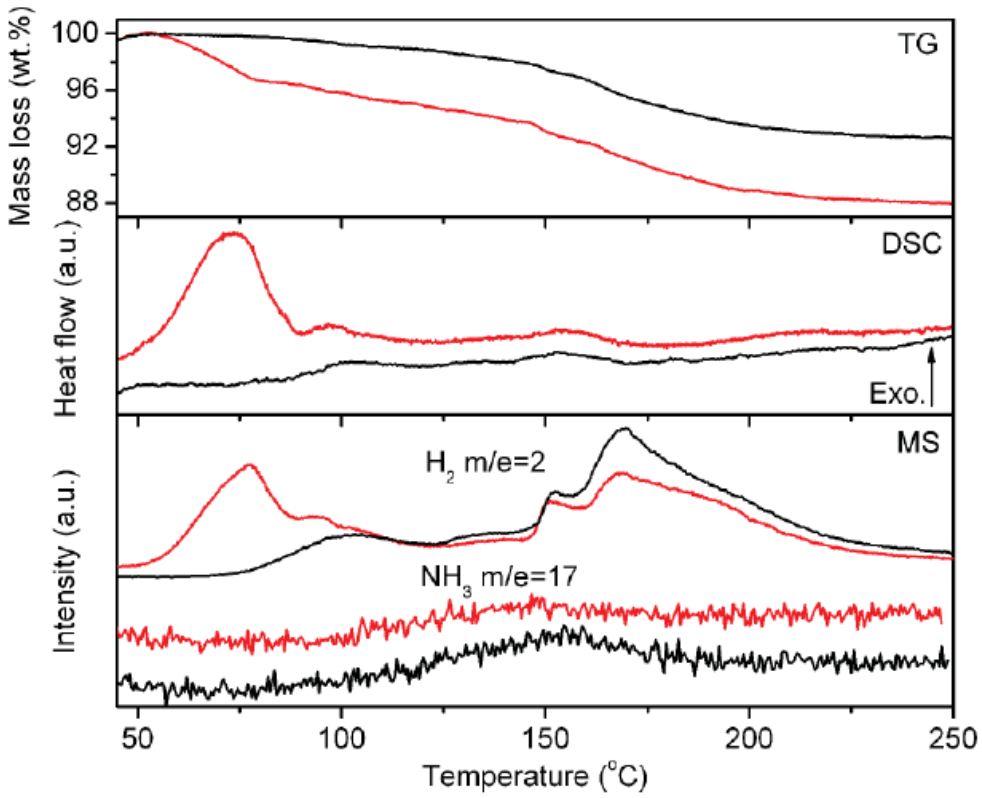

Fig. 11 TG/DSC/MS profiles of the $NaMg(NH_2BH_3)_3$ samples : post millied (red lines) and post-treated at 45 °C (black lines) [49]

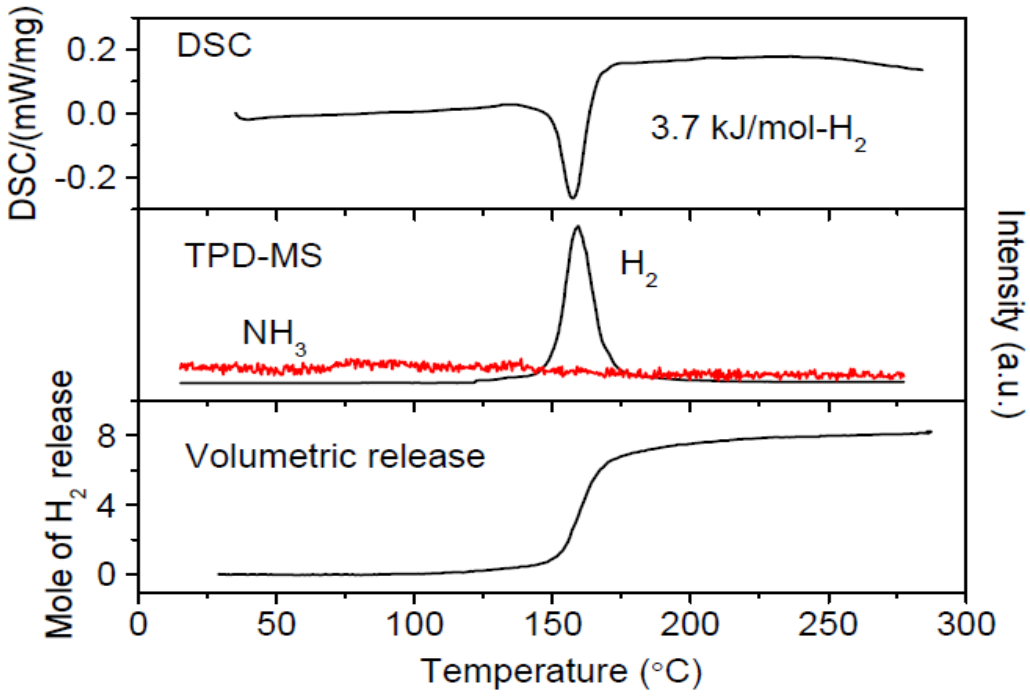

Fig. 12 TG/DSC/MS profiles of the $Na_2Mg(NH_2BH_3)_4$ sample [48]

The reason for change in the heat of reaction from exothermic to endothermic is due to the difference in enthalpy of formation of the substance. Figure 13 shows the change of enthalpy calculated. In case of AB alone, since the enthalpy after decomposition is smaller than the enthalpy of AB, the decomposition reaction proceeds with exothermic. However, dual-metal amidoborane could have a smaller than the enthalpy of decomposed compounds through reactant stabilization. Thus, both amidoboranes showed the potential of re-hydrogenation.

In the crystal structure of dual-metal amidoborane, the crystal structure analysis of $NaMg(NH_2BH_3)_3$ failed. However, they assumed that the following reactions (1-10) would occur to form $NaMg(NH_2BH_3)_3$.

$$3NH_3BH_3 + NaMgH_3 \rightarrow NaMg(NH_2BH_3)_3 + 3H_2 \qquad (1\text{-}10)$$

On the other hand, the crystal structure of $Na_2Mg(NH_2BH_3)_4$ was analyzed by X-ray diffraction techniques. It was identified from the data as having the space group $I4_1/a$ and approximate lattice parameters a = 9.415 Å and c = 12.413 Å.

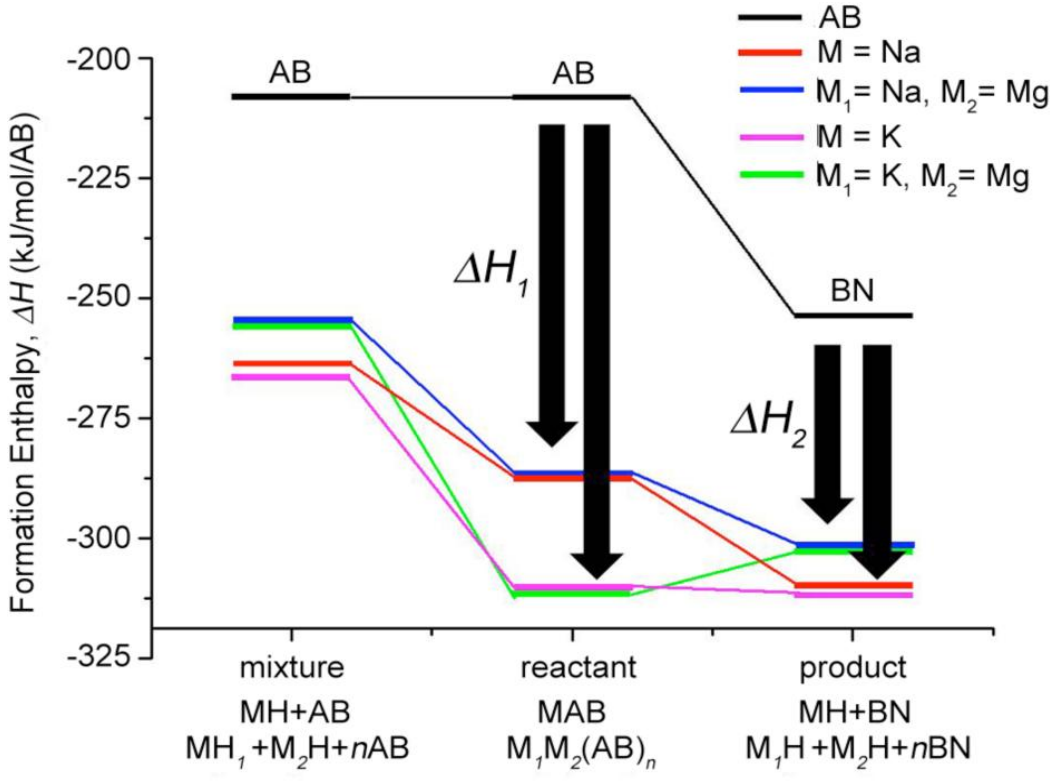

Fig. 13 Reduction of dehydrogenation exothermicity via reactant stabilization approach [48]

1.3.4 Aluminum hydride

Aluminum hydride (AlH_3) is an ideal off-board hydrogen storage material because of its high hydrogen capacities (10.1 mass% and 149 g H_2/L) and low desorption temperature (< 100 °C). [52] However, its desorption kinetics is not enough to meet the targets for practical applications. [53] Although AlH_3 is thermodynamically metastable at room temperature, it has been suggested that the surface Al_2O_3 film on AlH_3 particle would inhibit the spontaneous decomposition at room temperature. [54] Ball-milling can enhance the desorption kinetics of AlH_3, likely due to an increase of oxide free surfaces on AlH_3 particles. [54, 55] However, the mechanistic study showed that the real reason for the enhancement would be the small amount of desorption during ball-milling. [56, 57] The formation of metallic Al particles on the hydride surface would serve as channels for the enhanced desorption and reduce the incubation period. In addition, doping additives is one of the common strategies to enhance the kinetics of AlH_3. For instance, reactive hydride composites composed of AlH_3 and other hydrides (MgH_2 [58, 59], $LiBH_4$ [60], $MgCl_2$ [61] *etc.*) have been synthesized and their hydrogen desorption properties have been investigated. Also, Ti is a well-known and effective catalyst for AlH_3. The measurable enhancement of kinetics was observed by doping $TiCl_3$ with just a few ppm levels in solution during the AlH_3 synthesis. [57]

Nb-based additives have been considered as effective dopants to improve hydrogen sorption reactions of hydrogen storage materials. For instance, Nb_2O_5 is a well-known catalyst for hydrogen absorption and desorption reactions of MgH_2. [62-65] The composite, MgH_2 and 1 mol% Nb_2O_5 milled for 20 h, was able to absorb -4.5 mass% of hydrogen within 15 s at room temperature under lower pressure than 1.0 MPa and desorb -6.0 mass% of hydrogen at 160 °C. [63] Also, NbF_5 is also an effective dopant for various kinds of hydrogen storage materials, such as MgH_2 [66, 67], alanate [68, 69] and borohydride [70] system. The composite, MgH_2 and 2 mol% NbF_5 milled for 5 h, was able to absorb -5.0 mass% of hydrogen in 12 s and desorb -4.4 mass% of hydrogen in 10 min at 300 °C. [66] Hydrogen desorption properties of MgH_2-AlH_3 nanocomposites were investigated in the previous study, where the addition of just 1 mol% NbF_5 remarkably destabilized γ-AlH_3 in the composite and led to its decomposition at room temperature. [59]

1.4 Objective

Ammonia borane (NH_3BH_3) and Aluminum hydride (AlH_3) were selected from the DOE as high capacity hydrogen storage materials. However, each material has problems and cannot be used as it is.

In the case of NH_3BH_3, it has two problems to be realized as a hydrogen storage material. One is the reversibility for hydrogen desorption and absorption. NH_3BH_3 decomposes with releasing hydrogen through an exothermic reaction which means it is irreversible in thermodynamic principles. The other is the emission of by-product gases, such as ammonia and borazine, which make significant damage on fuel cells. These gases are generated in a complicated decomposition process of NH_3BH_3. In order to solve these problems, many studies have been conducted. Among them, dual-metal amidoborane is a thermodynamically stable material, and its de-hydrogenation reaction is expected to occur with endothermic reaction. In the previous studies, endothermic hydrogen release reactions were reported in two kinds of Na-Mg amidoboranes, $NaMg(NH_2BH_3)_3$ and $Na_2Mg(NH_2BH_3)_4$. However, the decomposition reactions of Na-Mg amidoboranes were not sufficiently understood. In this thesis, we made an attempt to synthesize $Na_2Mg(NH_2BH_3)_4$ and $NaMg(NH_2BH_3)_3$ by ball-milling of NH_3BH_3, MgH_2 and $NaNH_2$. Then, we investigated its reaction process by thermal and structure analyses. By comparing the process of $Na_2Mg(NH_2BH_3)_4$ and $NaMg(NH_2BH_3)_3$ which were synthesized by the same method, we proposed a hydrogen release process of Na-Mg amidoborane. The objective of the thesis lies in the following points.

(1) Investigation of facile synthesis method of dual-metal amidoboraen
(2) Investigation of the hydrogen desorption processes of Na-Mg amidoborane by comparing the $Na_2Mg(NH_2BH_3)_4$ and $NaMg(NH_2BH_3)_3$
(3) Investigation of re-hydrogenation of $Na_2Mg(NH_2BH_3)_4$ for the improvement of ammonia borane

In the case of AlH_3, the hydrogen release kinetics of AlH_3 is a problem. Due to the presence of a surface Al_2O_3 film on AlH_3 particles, a temperature of 140°C is required for hydrogen release. Among the various ways to improve the problem, I used Nb-based additives. In the previous study, the addition of 1 mol% NbF_5 to MgH_2-AlH_3

composites resulted in its decomposition at room temperature. However, the effect of Nb-based additives on AlH_3 has not been reported. In the present study, Nb, Nb_2O_5, and NbF_5 (hereinafter called "Nb species") were doped with α-AlH_3 (the most stable phase of AlH_3) and their hydrogen desorption properties and distribution states of Nb species were analyzed. In addition, the chemical bonding state of Nb species was further investigated in the NbF_5-doped AlH_3 and the reaction process was proposed.The objective of the thesis lies in the following points.

(1) Improvement of the dehydrogenation reaction kinetics of AlH_3 by adding Nb species

(2) Clarification of the additive effect of Nb species

References

1. Handbook of chemistry and physics, CRC, 2005
2. A. Züttel *et al*., *Phil. Trans. R. Soc. A* 368 (2010) 3329–3342
3. A. Züttel *et al*., *Naturwissenschaften* 91 (2004) 157–172
4. L. Schlapbach *et al*., *Nature*, 414 (2001) 353-358
5. B.C.R. Ewan *et al*., *Int. J. Hydrogen Energy* 30 (2005) 809-819
6. T.Q. Hua *et al*., *Int. J. Hydrogen Energy* 36 (2011) 3037-3049
7. M. Felderhoff *et al*., *Phys. Chem. Chem. Phys.* 9 (2007) 2643–2653.
8. A. Léon *et al*., Hydrogen technology, in Mobile and Portable Applications, Springer-Verlag, Berlin, Heidelberg, 2008
9. Recommended Best Practices for Characterizing Engineering Properties of Hydrogen Storage Materials, 2013
10. Targets for Onboard Hydrogen Storage Systems for Light-Duty Vehicles, DOE, 2009
11. https://www.nedo.go.jp/content/100642946.pdf
12. S. McWhorter *et al.*, *Crystals* 2 (2012) 413-445;
13. L. Schlapbach *et al.*, Hydrogen in Metal, in Electronic and Magnetic Properties of Metals and Ceramics Part 11, vol. 3B, VCH, Weinheim, 1994
14. Y. Fukai, K. Tanaka, H. Uchida, Hydrogen and Metals, Uchida Rokakuho Publishing co., Ltd., 2002
15. J. Graetz *et al., J.Alloys Compd.* 424 (2006) 262–265
16. Lea Fohlmeister *et al.*, *Aust. J. Chem.* 68 (2015) 1190–1201
17. G. Libowitz, The Solid-State Chemistry of Binary Metal Hydrides, W.A. Benjamin, New York, 1965
18. H. Saitoh *et al*., *JALCOM* 496 (2010) L25-L28
19. F. Schüth *et al., Chem. Comm.* (2004) 2249-2258
20. Borislav Bogdanovic *et al., JALCOM* 253-254 (1997) 1-9
21. Jun Chen *et al., J. Phys. Chem. B* 105 (2001) 11214-11220
22. H. Morioka *et al., JALCOM* 353 (2003) 310–314
23. H. Schlesinger *et al., J. Am. Chem. Soc.* 61 (1939) 536
24. A. Züttel *et al*., *Journal of Power Sources* 118 (2003) 1–7

25. H.-W. Li *et al*., D *Acta Materialia* 56 (2008) 1342–1347
26. K. Miwa *et al., PHYSICAL REVIEW B* 74 (2006) 155122
27. E. Jeon *et al., JALCOM* 422 (206) 273-275
28. Frances H. *Dalton Trans. (*2007) 2613–2626
29. G. Wolf *et al*., *Thermochimica Acta* 343 (2000) 19-25
30. Radu Custelcean *et al., Chem. Rev.* 101 (2001) 1963-1980
31. Z. XIONG *et al., Nat. Mater.* 7 (2007) 138–141.
32. F. Baitalow *et al., Thermochimica Acta* 391 (2002) 159-168
33. Zhang-Hui Lu *et al., J. Mater. Chem*., 22 (2012) 5065
34. Brian L. Conley et al., *J. Am. Chem. Soc.* 133 (2011) 14212–14215
35. Z. Tang *et al*., *Angew. Chem.* 52 (2013) 5832 –5835
36. J. Luo *et al*., *Phys. Chem. C.* 120, 33 (2016) 18386−18393
37. H.I. Schlesinger *et al*., *Journal of the American Chemical Society* 60, 2 (1938) 290-299
38. A.G. Myers *et al*., *Tetrahedron Letters* 37, 21 (1996) 3623-3626,
39. X. Kang *et al*., *Advanced Materials* 20, 14 (2008) 2756-2759,
40. H. Wu *et al*., *Journal of the American Chemical Society* 130, 44 (2008) 14834-14839
41. Nikola Biliskov *et al*., *Chemistry A European Journal* 23, 64 (2017) 16274-16282
42. Y. Nakagawa *et al*., *J. Mater. Chem. A.* 2 (2014) 3926-3931
43. W.Chen *et al*., *Sci. China chem.* 58 (2015) 169-173
44. Himashinie V. K. *J. AM. CHEM. SOC.* 132 (2010) 11836–11837
45. Zhitao Xiong *et al*., *Energy Environ. Sci* 1 (2008) 360–363
46. Karol J. Fijalkowski *et al.*, Dalton Trans. 40 (2011) 4407
47. H. Wu *et al.*, *Chem. Commun.* 47 (2011) 4102–4104,
48. Y. S. Chua *et al.*, *Chem. Mater.* 24, 18 (2012) 3574−3581
49. X. Kang *et al., Dalton Trans.* 40 (2011) 3799-3801
50. Iurii Dovgaliuk *et al., Chem. Eur. J.* 21 (2015) 14562 – 14570
51. Rafał Owarzany *et al.*, Mono- and Bimetalic Amidoboranes, *Crystals* 6 (2016) 88
52. J. Graetz, *ISRN Materials Science* 2012 (2012) 863025
53. J. Graetz, *et al., J. Alloys Comp.* 446-447 (2007) 271-275
54. G. Sandrock, *et al., J. Alloys Comp.* 421 (2006) 185-189

55. Y. Nakagawa *et al., J. Alloys Comp.* 580 (2013) S163-S166
56. I. Gabis *et al., J. Alloys Comp.* 509S (2011) S671-S674
57. J. Graetz *et al., J. Alloys Comp.* 509S (2011) S517-S528
58. H. Liu *et al., Phys. Chem.* C 118 (2014) 37-45
59. H. Liu *et al., J. Phys. Chem. C* 118 (2014) 18908-18916
60. H. Liu *et al., Int. J. Hydrogen Energy* 41 (2016) 22118-22127
61. C. W. Duan *et al., Phys. Chem. Chem. Phys.* 17 (2015) 22152-22159
62. G. Barkhordarian *et al., J. Alloys Comp.* 364 (2004) 242-246
63. N. Hanada *et al., J. Alloys Comp.* 420 (2006) 46-49
64. T. Ma *et al., J. Phys. Chem.* C 117 (2013) 10302-10307
65. T. Kimura *et al., Int. J. Hydrogen Energy* 38 (2013) 13728-13733
66. Y. Luo *et al., J. Alloys Comp.* 453 (2008) 138-142
67. N. Recham *et al., J. Alloys Comp.* 464 (2008) 377-382
68. M. Ismail *et al., Int. J. Hydrogen Energy* 35 (2010) 2361-2367
69. J. Mao *et al., Int. J. Hydrogen Energy* 36 (2011) 14503-14511
70. H. Kou *et al., Int. J. Hydrogen Energy* 39 (2014) 11675-11682

Chapter 2

Synthesis of various kinds of dual-metal amiboborane

2.1 Background and purpose

As mentioned in chapter 1, various types of dual-metal amidoborane have been studied from 2011 by Fijalkowsi Kj. [1] Table 2-1 shows all types of dual-metal amidoboranes reported. [1-9]

Table 2-1All types of dual-metal amidoboranes

Chemical formula	Reaction equation	Synthetic method
$LiNa(NH_2BH_3)_2$	$LiH + NaH + 2NH_3BH_3 \rightarrow LiNa(NH_2BH_3)_2 + 2H_2$	Ball-milling [1]
$LiNa(NH_2BH_3)_2$	$LiAB + NaAB \rightarrow LiNa(NH_2BH_3)_2$	In THF solvent [2]
$LiAl(NH_2BH_3)_4$	$LiAlH_4 + 4NH_3BH_3 \rightarrow LiAl(NH_2BH_3)_4 + 4H_2$	In THF solvent [3]
$NaAl(NH_2BH_3)_4$	$NaAlH_4 + 4NH_3BH_3 \rightarrow NaAl(NH_2BH_3)_4 + 4H_2$	Ball-milling [4]
$NaMg(NH_2BH_3)_3$	$NaMgH_3 + 3NH_3BH_3 \rightarrow NaMg(NH_2BH_3)_3 + 3H_2$	Ball-milling [5]
$Na_2Mg(NH_2BH_3)_4$	$2NaH + MgH_2 + 4NH_3BH_3 \rightarrow Na_2Mg(NH_2BH_3)_4 + 4H_2$	Ball-milling [6]
$Na_2Mg(NH_2BH_3)_4$	$2Mg(NH_2BH_3)_2{\cdot}NH_3 + 2\ NaH \rightarrow Na_2Mg(NH_2BH_3)_4 + Mg(NH_2)_2 + 2H_2$	Ball-milling [7]
$K_2Mg(NH_2BH_3)_4$	$2Mg(NH_2BH_3)_2{\cdot}NH_3 + 2\ KH \rightarrow K_2Mg(NH_2BH_3)_4 + Mg(NH_2)_2 + 2H_2$	Ball-milling [7]
$KMg(NH_2BH_3)_3$	$KMgH_3 + 3NH_3BH_3 \rightarrow KMg(NH_2BH_3)_3 + 3H_2$	Ball-milling [8]
$RbMg(NH_2BH_3)_3$	$RbMgH_3 + 3NH_3BH_3 \rightarrow RbMg(NH_2BH_3)_3 + 3H_2$	Ball-milling [8]
$Li_2Mg(NH_2BH_3)_4$	$2LiH + MgH_2 + 4NH_3BH_3 \rightarrow Li_2Mg(NH_2BH_3)_4 + 4H_2$	Ball-milling [9]

As shown in table 2-1, nine types of dual-metal amidoborane were found. Among them, there are some that are considered to release hydrogen with endothermic reaction. However, it is $NaMg(NH_2BH_3)_3$ and $Na_2Mg(NH_2BH_3)_4$ that are clearly visible.

In previous study, synthesizing $NaMg(NH_2BH_3)_3$ is very complicated and take a long time (milling $3NH_3BH_3$ and $NaMgH_3$ for 1 hour followed by annealing at 45 ºC overnight). [5] Therefore, the purpose of this chapter is to investigate facile synthesis method of $NaMg(NH_2BH_3)_3$ and to clarify their formation mechanism.

2.2 Experimental procedure

2.2.1 Sample synthesis

2.2.1.1 Composite of $NH_3BH_3 + MgH_2 + NaX$ (X = H, NH_2, BH_4)

Figure 2-1 shows a method of synthesizing samples. NH_3BH_3 (Sigma-Aldrich, purity 97%, AB), MgH_2 (Alfa Aesar, purity 98%), NaH (Sigma-Aldrich, purity 55-65% (moistened with oil)), $NaNH_2$ (Sigma-Aldrich, purity 98%) and $NaBH_4$ (Sigma-Aldrich, purity 98%) were weighed to be totally 300 mg, and mixed at molar ratios of NH_3BH_3 : MgH_2 : NaX = 3 : 1 : 1 by using planetary ball-mill apparatus (Fritsch Pulverisette 7). The milling was performed using steel balls of total 21 g under 1.0 MPa of H_2 atmosphere, at 400 rpm for 2 hours, with 30 min operation and 15 min interval. All sample handlings were performed in a glove box with Ar atmosphere.

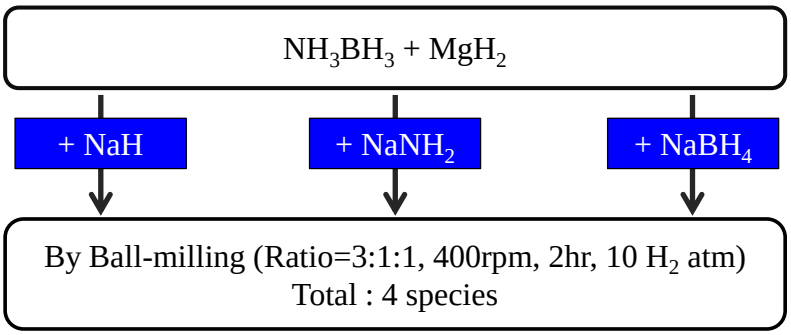

Fig. 2-1 Method of synthesizing samples

2.2.1.2 Composite of $NH_3BH_3 + MgH_2 + NaNH_2$

NH_3BH_3 (Sigma-Aldrich, purity 97%), MgH_2 (Alfa Aesar, purity 98%) and $NaNH_2$ (Sigma-Aldrich, purity 98%) were weighed to be totally 300 mg, and mixed at molar ratios of NH_3BH_3 : MgH_2 : $NaNH_2$ = 3 : 1 : 1 by using planetary ball-mill apparatus (Fritsch Pulverisette 7). The milling was performed under 1.0 MPa of H_2 atmosphere, at 400 rpm for 2, 12 and 24 hours, respectively.

2.2.2 Characterization

The crystalline phases were identified by powder X-ray diffraction (PANalytical, X'Pert-Pro with Cu Kα radiation). The outputs of the filament voltage and current were 40 kV and 200 mA, respectively. The sample was set on a glass plate and covered with a polyimide sheet (Kapton, Du Pont-Toray Co. LTD) with grease (Apiezon, M&I material Ltd.) in glove box for avoiding the samples exposed to the air. The decomposition properties were evaluated by thermogravimetry and differential thermal analysis equipment (TG-DTA, Bruker 2000SA) and connected to a mass spectrometer (MS, ULVAC, BGM-102). The generated gas flows from the TG-DTA equipment to MS by He gas. The flow rate of He gas was 300mL/min. The temperature range for heating sample was from room temperature to 300 ºC with a heating rate of 5 ºC /min.

2.3 Results and discussions

2.3.1 Composite of NH_3BH_3 + MgH_2 + NaX (X = H, NH_2, BH_4)

The synthesis of $NaMg(NH_2BH_3)_3$ was confirmed by the type of NaX (X = H, NH_2, BH_4). Figure 2-2 shows the XRD results of each sample. $NaMg(NH_2BH_3)_3$ was prepared by the method of the previous study.[5] The result of the sample to which NaH was added is shown in Fig. 2-2 a). There is unknown peak on the low angle side, which will be described in detail in chapter 4. As impurities other than $NaMg(NH_2BH_3)_3$, $NaNH_2BH_3$ and MgH_2 were confirmed. $NaNH_2BH_3$ is known to be generated in the reaction of NaH and AB from previous study. [10] MgH_2 is unreacted starting materials. Figure 2-2 b) shows the result of adding $NaNH_2$ and the same result as in Fig. 2-2 a) was obtained. However, the initial substances AB, MgH_2 and $NaNH_2$ were all detected because the time to complete reaction was insufficient. In Fig.2-2 c), the peaks of $NaMg(NH_2BH_3)_3$ were not confirmed. It was just a mixture of AB, MgH_2 and $NaBH_4$.

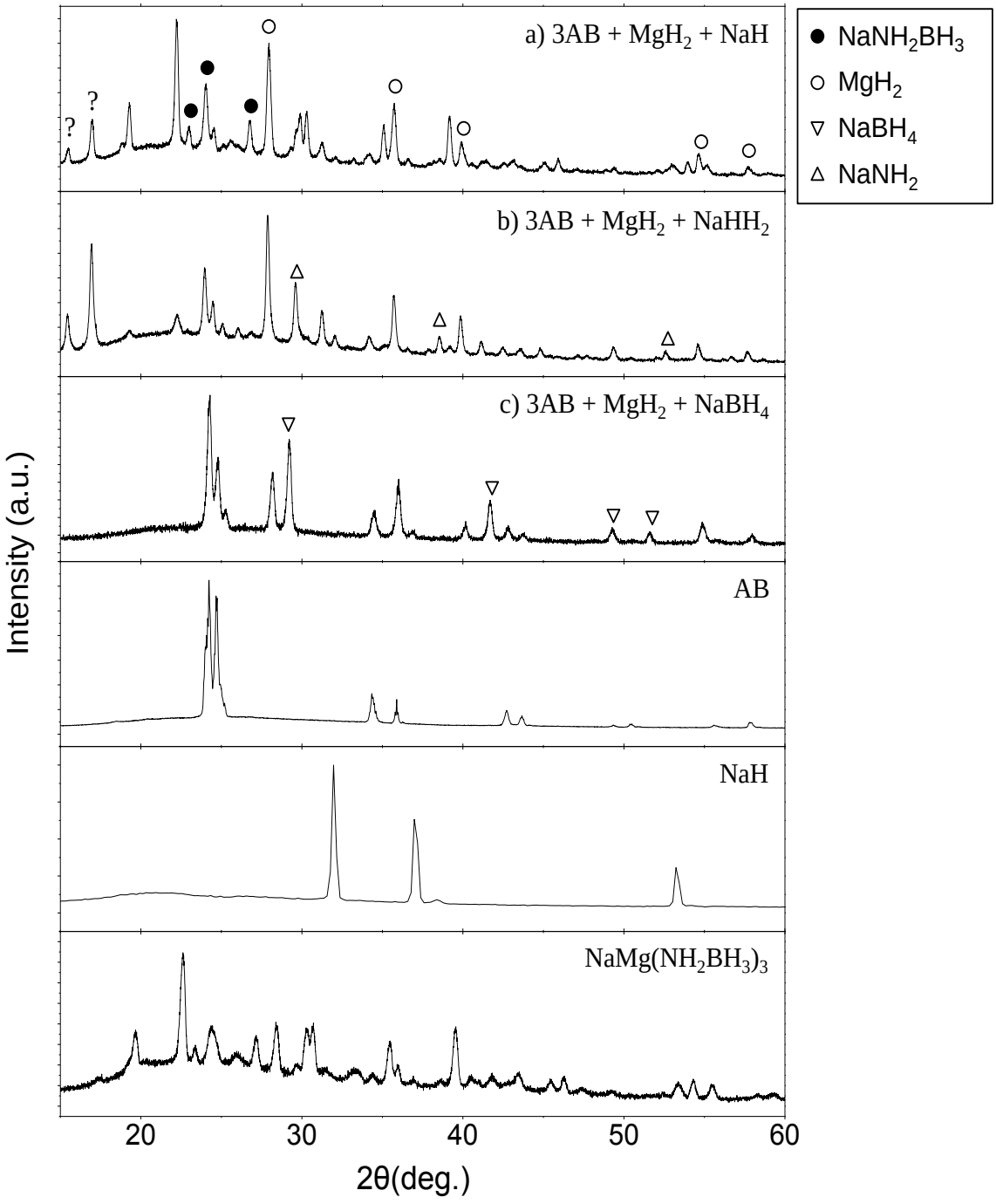

Fig. 2-2 XRD patterns of a) 3AB + MgH_2 + NaH, b) 3AB + MgH_2 + $NaNH_2$, c) 3AB + MgH_2 + $NaBH_4$, AB, NaH and $NaMg(NH_2BH_3)_3$ by the previously reported method in [5]

The reason why such a difference is obtained is considered to be due to the reactivity of NaX and AB. NaH and $NaNH_2$ react with AB to synthesize $NaNH_2BH_3$. [10, 11] In particular, $NaNH_2$ and AB react violently while forming foam when they are mixed with each other in powder. In contrast, $NaBH_4$ has low reactivity with AB. [12] The reason why the reactivity with AB is important is considered from the formation mechanism of $Mg(NH_2BH_3)_2$. [13] It is necessary to carry out heat treatment in order for MgH_2 and AB to react. The heat treatment loosens the bonding of AB to form bonding of Mg and nitrogen (in AB). Thus, the reaction of NaX (X = H or $NaNH_2$) with AB changes the structure of AB. Thereafter, it is considered that compounds produced from the reaction of NaX and AB reacts with MgH_2.

Figure 2-3 shows the MS profiles of each sample. This is the result of NaH, $NaNH_2$ and $NaBH_4$ respectively from left. The results of NaH show that the emission peak of hydrogen is complicated. This means that there is not a single phase emission, but multiple phases. There were also several compounds from the result of XRD. In particular, the release of diborane and ammonia is from the starting material AB. In the result of $NaNH_2$, the emission peaks of hydrogen were broad and complicated but the peak of by-product gas was not observed. From the results of XRD, ammonia and other by-product gases should be released as there were several compounds in the sample. This will be explained in detail in 2.3.2. The $NaBH_4$ results gave emission peaks from the mixture as well as the XRD results. The emission peaks of hydrogen and by-product gas are the same as typical AB decomposition reaction peaks. This means that the starting materials AB, MgH_2 and $NaBH_4$ form a mixture without forming new compounds.

Figure 2-4 shows the weight loss results of sample. From the sample with a largest mass change, it is the order of $NaBH_4$ (about 25 mass %), NaH (about 11 mass %) and $NaNH_2$ (about 5 mass %). These results are due to the amount of by-product gases as can be seen from Fig. 2-3. $NaBH_4$ with the largest amount of by-product gas evolved has a large mass change, and $NaNH_2$ with a small amount of by-product gas has a small mass change. In the case of AB alone, a mass change of about 50 mass % is observed due to by-product gas. In the case of $NaBH_4$ sample, the mass change is half that of AB alone because the content of AB is about 50%.

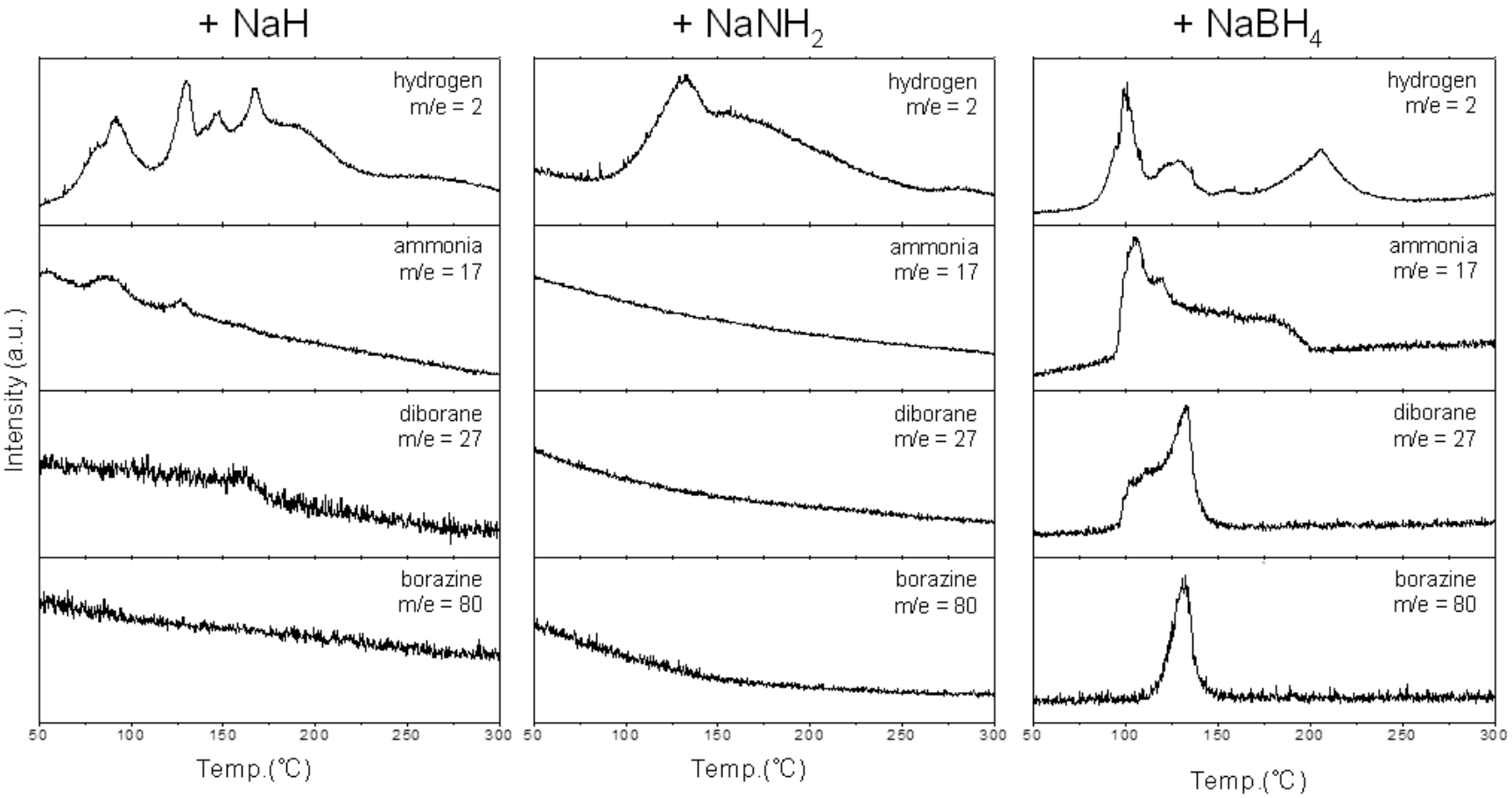

Fig. 2-3 MS profiles of samples from R.T. to 300 ºC (heating rate = 5 ºC / min)

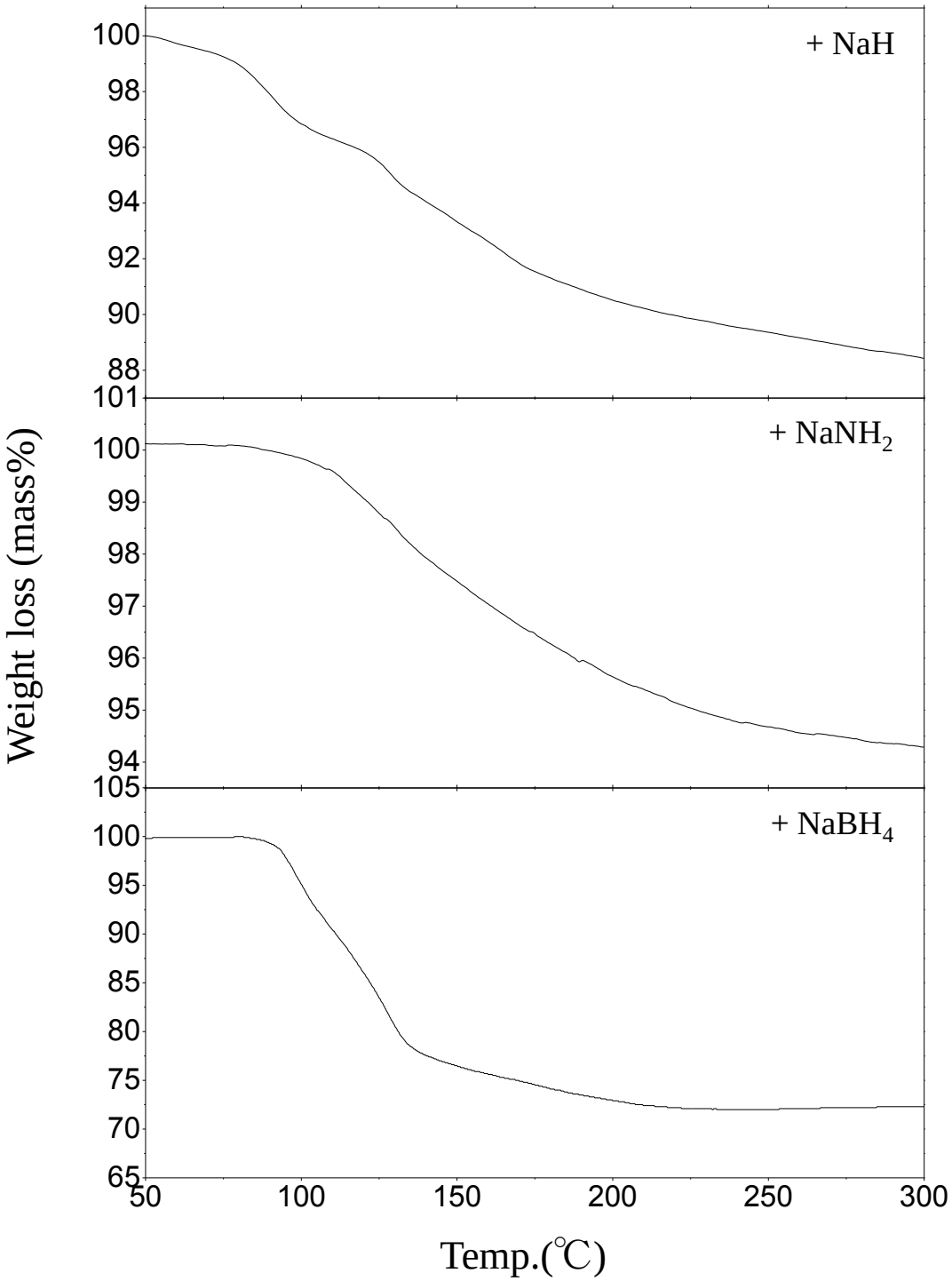

Fig, 2-4 TG profile of sample from R.T. to 300 ºC (heating rate = 5 ºC / min)

2.3.2 Composite of NH_3BH_3 + MgH_2 + $NaNH_2$

Among the samples mentioned in 2.3.1, $NaNH_2$ added samples which did not form compounds (*e.g.* $NaNH_2BH_3$ in NaH sample) other than $NaMg(NH_2BH_3)_3$ were prepared under three milling conditions. Figure 2-5 shows the XRD results of samples (milling condition = 2hr, 12hr). In the sample milled for 24 hours, XRD experiments could not be performed because the powder stuck to the milling pot or ball after milling. The reason is considered that the sample reacted too much due to the long milling time. As compared with Fig. 2-5 a), the sample milled for 12 hours did not show AB and $NaNH_2$ which are initial materials. This means that the sample reacts almost completely in 12 hours.

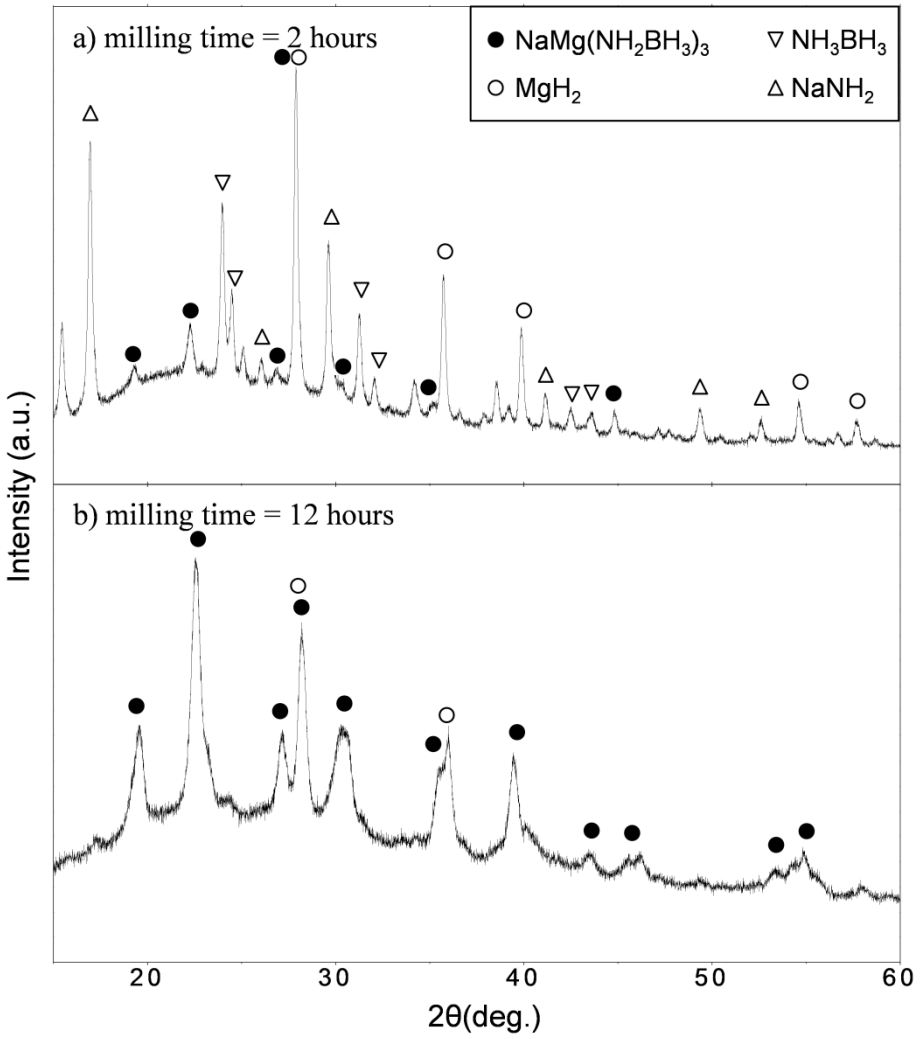

Fig. 2-5 XRD results of samples; a) milling time = 2 hours, b) milling time = 12 hours

2.4 Summary

In this chapter, a study on synthesis of $NaMg(NH_2BH_3)_3$ was performed with various starting materials and milling condition. We found that $NaMg(NH_2BH_3)_3$ was synthesized under the conditions of 3 AB + MgH_2 + NaH and 3 AB + MgH_2 + $NaNH_2$. In the combination of AB, MgH_2 and NaH, the $NaNH_2BH_3$ was synthesized in addition to $NaMg(NH_2BH_3)_3$. A milling time of 12 hours is required for the sample to react sufficiently.

References

1. Karol J. Fijalkowski *et al*., Na[Li(NH2BH3)2] - the first mixed-cation amidoborane with unusual crystal structure, *Dalton Trans*, 40 (2011) 4407
2. W. Li *et al*., Li-Na ternary amidoborane for hydrogen storage: experimental and first-principles study, *Dalton Trans*, 41 (2012) 4701 - 5072
3. J. Michael Hoy *et al*., Syntheses of Aluminum Amidotrihydroborate Compounds and Ammonia Triborane as Potential Hydrogen Storage Materials, *The Ohio State University*, 2010
4. Iurii Dovgaliuk *et al*., A Composite of Complex and Chemical Hydrides Yields the First Al-Based Amidoborane with Improved Hydrogen Storage Properties, *Chem. Eur. J.*, 21 (2015) 14562 - 14570
5. X. Kang *et al*., Combined formation and decomposition of dual-metal amidoborane $NaMg(NH_2BH_3)_3$ for high-performance hydrogen storage, *Dalton Trans*, 40 (2011) 3799
6. H. Wu *et al*., Sodium magnesium amidoborane: the first mixed-metal amidoborane, *Chem. Commun.*, 47 (2011) 4102 - 4104
7. Y. S. Chua *et al*., From Exothermic to Endothermic Dehydrogenation-Interaction of Monoammoniate of Magnesium Amidoborane and Metal Hydrides, *Chem. Mater.*, 24 (2012) 3574 - 3581
8. X. Kang *et al*., Efficient and highly rapid hydrogen release from ball-milled $3NH_3BH_3/MMgH_3$ (M = Na, K, Rb) mixtures at low temperatures, *international journal of hydrogen energy*, 37 (2012) 4259 - 4266
9. Nikola Biliskov *et al*., In-situ and Real-time Monitoring of Mechanochemical Preparation of Li2Mg(NH2BH3)4 and Na2Mg(NH2BH3)4 and their Thermal Dehydrogenation, *Chem. Eur. J.*, 23 (2017) 16274 - 16282
10. Z. Xiong *et al*., Synthesis of sodium amidoborane ($NaNH_2BH_3$) for hydrogen production, *Energy Environ. Sci.*, 1 (2008) 360 - 363
11. W. Chen *et al*., New synthetic procedure for $NaNH_2(BH_3)_2$ and evaluation of its hydrogen storage properties, *SCIENCE CHINA Chemistry*, 58 (2015) 169 - 173
12. L.H. Jepsen *et al*., Investigations of the thermal decomposition of $MBH_4–2NH_3BH_3$, M = Na, K, *JALCOM*, 580 (2013) 287 - 291

13. J. Luo *et al*., Synthesis, formation mechanism, and dehydrogenation properties of the long-sought $Mg(NH_2BH_3)_2$ compound, *Energy Environ. Sci*, 6 (2013) 1018

Chapter 3

Dehydrogenation processes of sodium-magnesium amidoborane ($NaMg(NH_2BH_3)_3$ and $Na_2Mg(NH_2BH_3)_4$)

3.1 Background and purpose

Na-Mg amidoborane is a thermodynamically stable material, and its de-hydrogenation reaction is expected to occur with endothermic reaction. [1-3] In the previous studies, endothermic hydrogen release reactions were reported in two kinds of Na-Mg amidoboranes, $NaMg(NH_2BH_3)_3$ and $Na_2Mg(NH_2BH_3)_4$. Thus, both amidoboranes showed the potential of re-hydrogenation. Although the crystal structure analysis of $NaMg(NH_2BH_3)_3$ failed, they assumed that the following reaction 3-1 would occur to form $NaMg(NH_2BH_3)_3$.

$$3NH_3BH_3 + NaMgH_3 \rightarrow NaMg(NH_2BH_3)_3 + 3H_2 \quad (3\text{-}1)$$

The obtained $NaMg(NH_2BH_3)_3$ showed the multiple decomposition steps and one of them showed the endothermic dehydrogenation. [3] On the other hand, the crystal structure of $Na_2Mg(NH_2BH_3)_4$ was analyzed by X-ray diffraction techniques. This phase also showed the endothermic dehydrogenation around 160 ºC. [2] It is interesting that two kinds of Na-Mg amidoboranes showed the endothermic dehydrogenation steps. However, the decomposition reactions of Na-Mg amidoboranes were not sufficiently understood. Thus, in order to clarify the endothermic dehydrogenation process, we investigated the decomposition properties of Na-Mg amidoborane. First, we made an attempt to synthesize $Na_2Mg(NH_2BH_3)_4$ and $NaMg(NH_2BH_3)_3$ by ball-milling of NH_3BH_3, MgH_2 and $NaNH_2$. Then, we investigated its reaction process by thermal and structure analyses. By comparing the process of $Na_2Mg(NH_2BH_3)_4$ and $NaMg(NH_2BH_3)_3$ which were synthesized by the same method, we proposed a hydrogen release process of Na-Mg amidoborane.

3.2 Experimental procedure

3.2.1 Sample synthesis

NH_3BH_3 (Sigma-Aldrich, purity 97%), MgH_2 (Alfa Aesar, purity 98%), and $NaNH_2$ (Sigma-Aldrich, purity 98%) were weighed to be totally 300 mg, and mixed at molar ratios of NH_3BH_3 : MgH_2 : $NaNH_2$ = 3 : 1 : 1 and 4 : 1 : 2 by using planetary ball-mill apparatus (Fritsch Pulverisette 7). The milling was performed using steel balls of total 21 g under 1.0 MPa of H_2 atmosphere, at 400 rpm for 12 hours, with 30 min operation and 15 min interval. In order to clarify the decomposition process, heat-treated samples were prepared by heating up to the hydrogen release temperature of each sample.

3.2.2 Characterization

The decomposition properties were evaluated by thermogravimetry and differential thermal analysis equipment (TG-DTA, Bruker 2000SA) and connected to a mass spectrometer (MS, ULVAC, BGM-102). The generated gas flows from the TG-DTA equipment to MS by He gas. The flow rate of He gas was 300mL/min. The temperature range for heating sample was from room temperature to 250 ºC with a heating rate of 5 ºC /min. The crystalline phases were identified by powder X-ray diffraction (XRD, PANalytical, X'Pert-Pro with Cu Kα radiation). The sample was set on a glass plate and covered with a polyimide sheet with grease in glove box for avoiding the samples from being exposed to the air. ^{11}B magic angle spin (MAS) NMR spectra was examined by using solid state nuclear magnetic resonance (NMR,Bruker, DSX-300) in a magnetic field of 7.1 T (300MHz). The ^{11}B spectra were referenced to $NaBH_4$ (-42.06 ppm). All of the samples were packed into 4mm ZrO_2 rotors under Ar atmosphere, and spun at a speed of 8 kHz. The vibrational properties were analyzed by fourier transform infrared (FTIR, JASCO, FT/IR-4600) spectroscopy with KBr plate.

3.3 Results and discussions

3.3.1 Decomposition process of the composite (NH_3BH_3:MgH_2:$NaNH_2$=3:1:1)

$NaMg(NH_2BH_3)_3$ was synthesized by milling NH_3BH_3, MgH_2 and $NaNH_2$ with a molar ratio of 3 : 1 : 1. Figure 3-1 shows the XRD patterns of the synthesized composite. Figure 3-1 (b) shows the XRD patterns of $NaMg(NH_2BH_3)_3$ prepared according to the reported method in [3] (milling $3NH_3BH_3$ and $NaMgH_3$ for 1 hour followed by annealing at 45 ºC overnight). In both XRD patterns, the peaks corresponding to the reported $Na_2Mg(NH_2BH_3)_4$ were observed, although the broadness of peaks was different. The reason why $Na_2Mg(NH_2BH_3)_4$ was synthesized while $NaMg(NH_2BH_3)_3$ should be produced will be described later in this chapter. The size of crystallite of Fig.3-1 (a) was smaller than that of Fig.3-1 (b), probably due to the long milling time and no heat treatment in the case of Fig.3-1 (a). Meanwhile, the initial substance of MgH_2 was identified in Fig.3-1 (a). Also the peaks of NH_3BH_3 and $NaMgH_3$ were identified in Fig.3-1 (b). Thus, the unreacted starting materials remained in both composites.

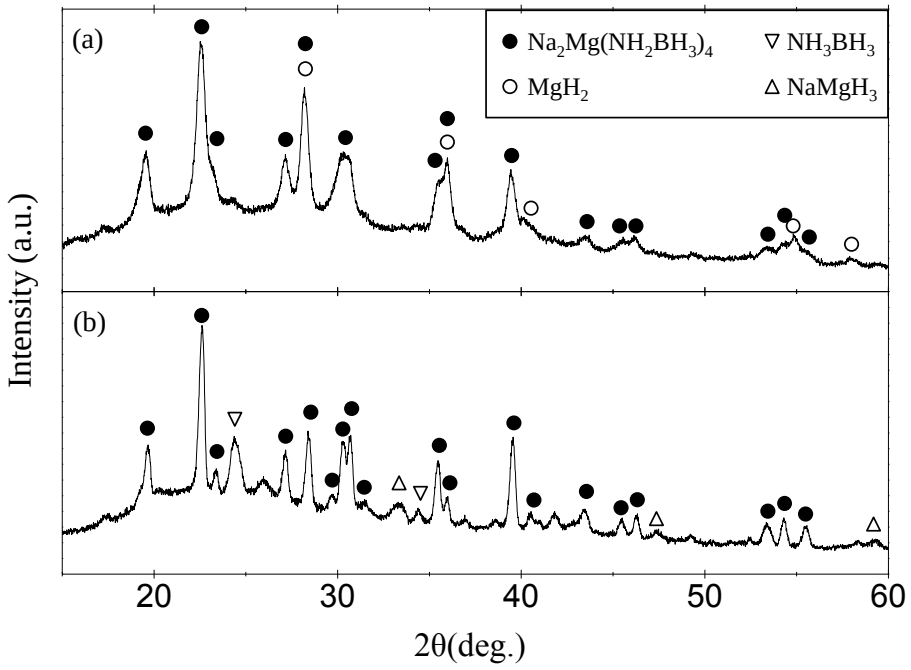

Fig.3-1 XRD patterns of (a) composite prepared by ball-milling (NH_3BH_3 : MgH_2 : $NaNH_2$ = 3 : 1 : 1, 12 hrs), (b) composite prepared by the previously reported method in [3]

Figure 3-2 shows the results of thermal analysis of the composite synthesized by our method and previously reported method in [3] (corresponding to the sample of Figure 3-1 (a), (b)). Total weight loss of both samples was about 11 wt.%, due to the gas emission of hydrogen and ammonia as shown in the result of Fig. 3-2 (c) and (d). In the previous study[3], the DSC profile showed small peaks because the sample amount for measurement was small. However, in this study, DTA peaks appeared more clearly by increasing the sample amount. We have checked several other kinds of gas emission such as borazine and diborane, which have been released from NH_3BH_3 itself, and no other gases have been detected. In Fig.3-2 (a) and (b), a few exothermic reactions and one endothermic reaction (indicated by arrows) were observed, which corresponds to hydrogen release steps in Fig.3-2 (c) and (d). The hydrogen release peak temperature in Fig. 3-2 (c) shown by the black circle is the same as the heat treatment temperature.

Next, in order to investigate the crystalline phases of each decomposition step, we performed XRD on the composites (NH_3BH_3 : MgH_2 : $NaNH_2$ = 3 : 1 : 1) heat-treated at 100, 130, 155 and 190 ºC. The temperature was determined by each hydrogen desorption step obtained from black circle in Fig.3-2 (c). The results of XRD for the samples as ball-milled and heat-treated at 100, 130, 155, 190 ºC are shown in Fig.3-3. In the profiles of heat-treated at 100 ºC, 130 ºC, and 155 ºC, unknown peaks have appeared around 25 degree of 2θ. The $NaBH_4$ peaks have appeared at 155 ºC and 190 ºC. This result was consistent with the previous report. [1] The milled composite contained large amount of unreacted MgH_2. The unreacted MgH_2 was also observed in the patterns of all the heat-treated samples.

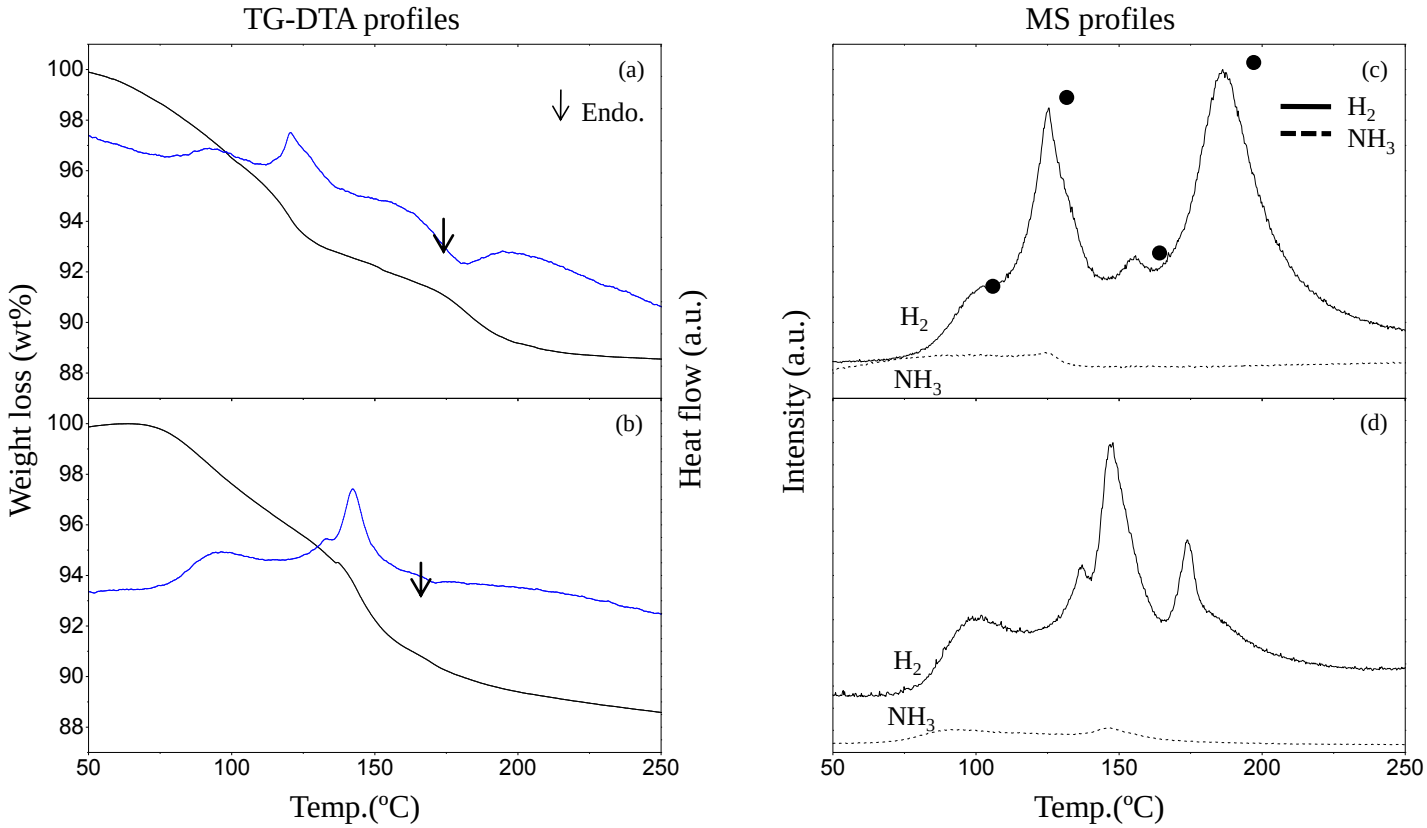

Fig.3-2 TG-DTA profiles of (a) composite prepared by ball-milling (NH_3BH_3 : MgH_2 : $NaNH_2$ = 3:1:1, 12 hrs) and (b) composite prepared by the previously reported method in [3] (Black line : weight loss, blue line : heat flow), MS profiles of (c) composite prepared by ball-milling (NH_3BH_3 : MgH_2 : $NaNH_2$ = 3:1:1, 12 hrs) and (d) composite prepared by the previously reported method in [3] (Solid line : hydrogen, dashed line : ammonia), Heating rate = 5ºC /min, He flow. The black circle corresponds to annealing temperature used for Fig. 3-3.

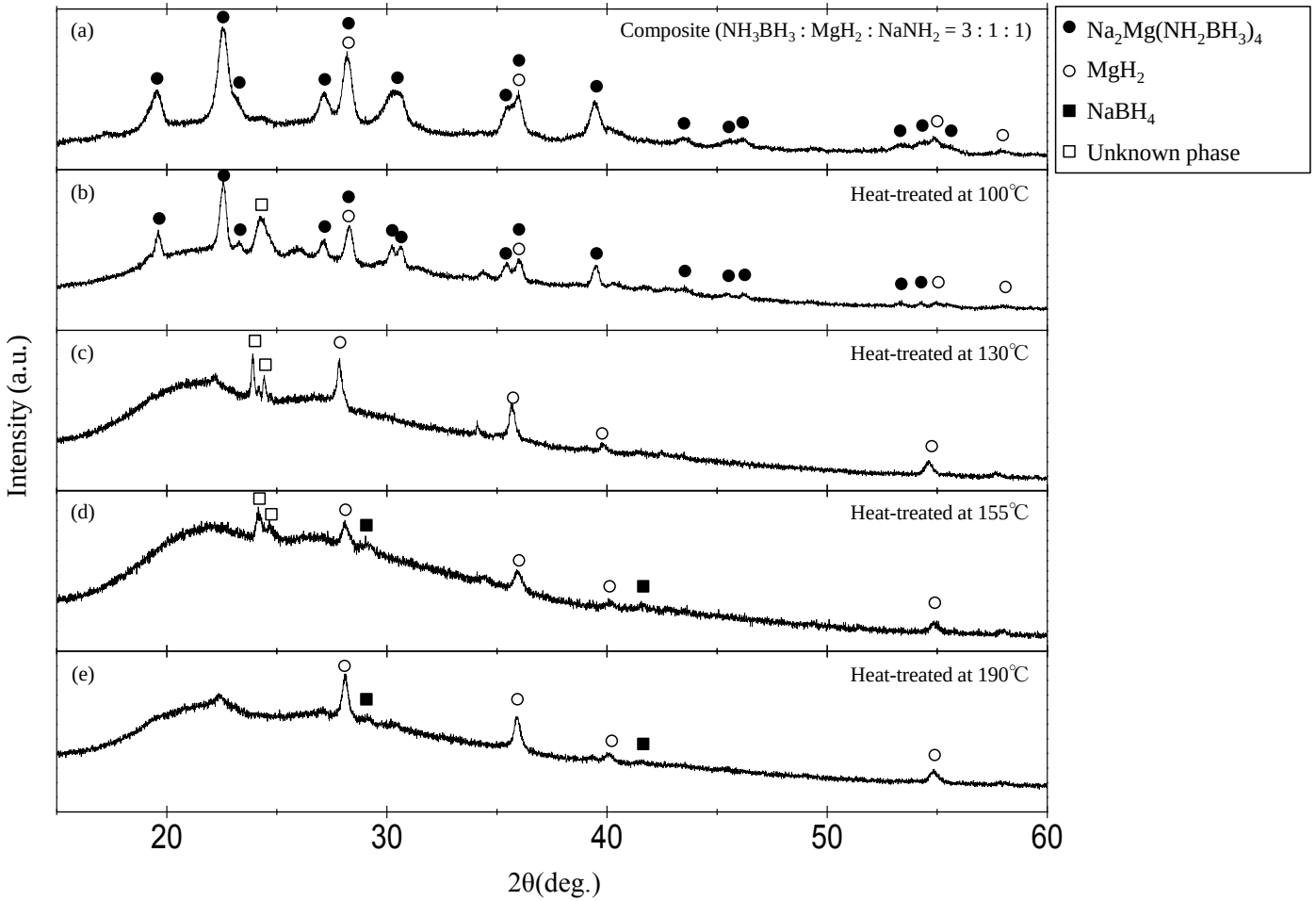

Fig.3-3 XRD patterns of (a) composite (NH_3BH_3 : MgH_2 : $NaNH_2$ = 3 : 1: 1) at R.T. (reference pattern from Fig. 3-1 (a)), (b) heat-treated at 100 ºC, (c) heat-treated at 130 ºC, (d) heat-treated at 155 ºC, (e) heat-treated at 190 ºC

Figure 3-4 shows the ^{11}B MAS NMR spectra of composites. The peak around -25.0 ppm was observed in the synthesized composite, which can be assigned to $Na_2Mg(NH_2BH_3)_4$ (-24 ppm) [2]. The observed peak may contain the residual AB species, whose peak position is reported at -25.3 ppm [4]. The sample has a single boron site ([NBH_3]), indicating that the asymmetric peak shape of AB is influenced by the nuclear quadrupolar interaction. In Fig. 3-4 (c), two additional broad peaks were observed at around -18 ppm and 20 ppm, respectively. The peak formed at -18 ppm is the peak of [BH_2]. And the peak formed at 20 ppm can be assigned to three-fold boron ([BN_3] or [N_2BH] species) as in hexagonal BN (h-BN) or polyborazilene.[5] This broad peak is a peak generated when $Na_2Mg(NH_2BH_3)_4$ decomposes, and thus became stronger as the reaction progresses. The peak at -42 ppm in Fig. 3-4 (c)-(e) can be assigned to [BH_4] species in $NaBH_4$ [6]. This result is consistent with the formation of $NaBH_4$ in the XRD profiles of Fig. 3-3.

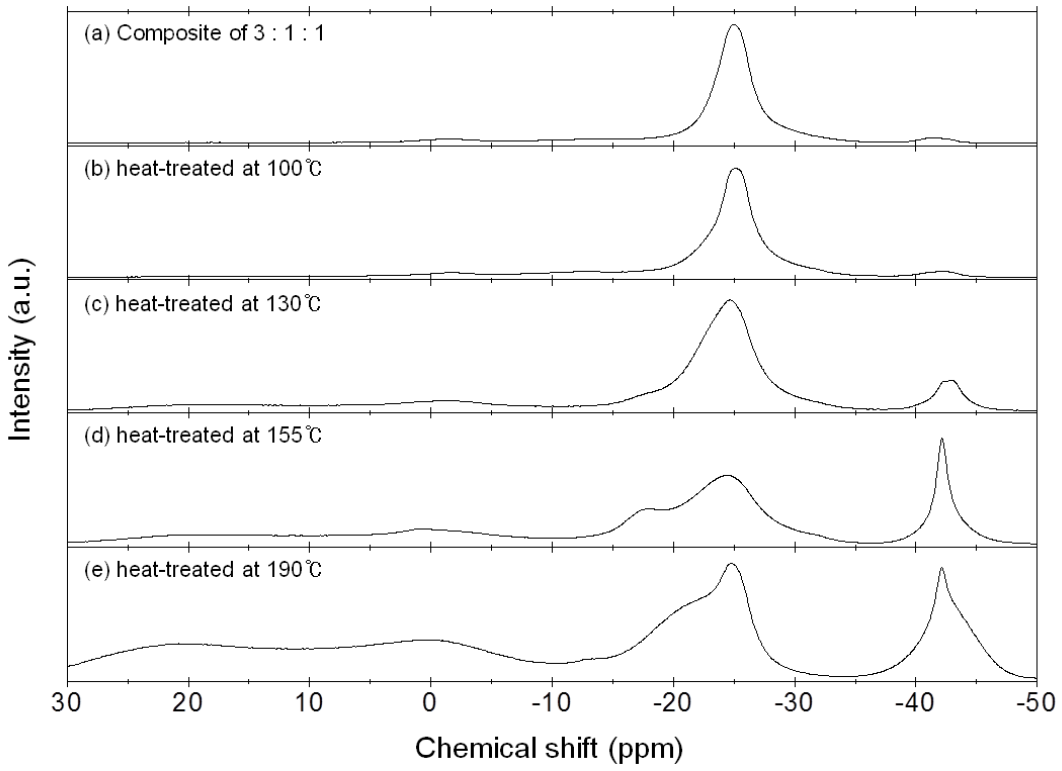

Fig.3-4 Solid state ^{11}B NMR spectra of (a) Composite of NH_3BH_3 : MgH_2 : $NaNH_2$ = 3 : 1 : 1 at R.T., (b) heat-treated at 100 ºC, (c) heat-treated at 130 ºC, (d) heat-treated at 155 ºC, (e) heat-treated at 190 ºC

Figure 3-5 shows the FTIR spectra of each sample. This shows that the substitution of amine H by the more electron donating Na and Mg cations results in bonding structure changes. The N-H stretch in Fig. 3-5 (a), peaks were at 3337, 3301, 3285 and 3256 cm^{-1}. These peaks were at positions corresponding to AB and $Na_2Mg(NH_2BH_3)_4$. [7, 2] As the temperature increased, the N-H bond changed from NH_2 to NH. In Fig. 3-5 (a), B-N stretches changed to blue-shift relative to the original AB. This means that the weakened B–H bonds and significantly strengthened B–N bonds.

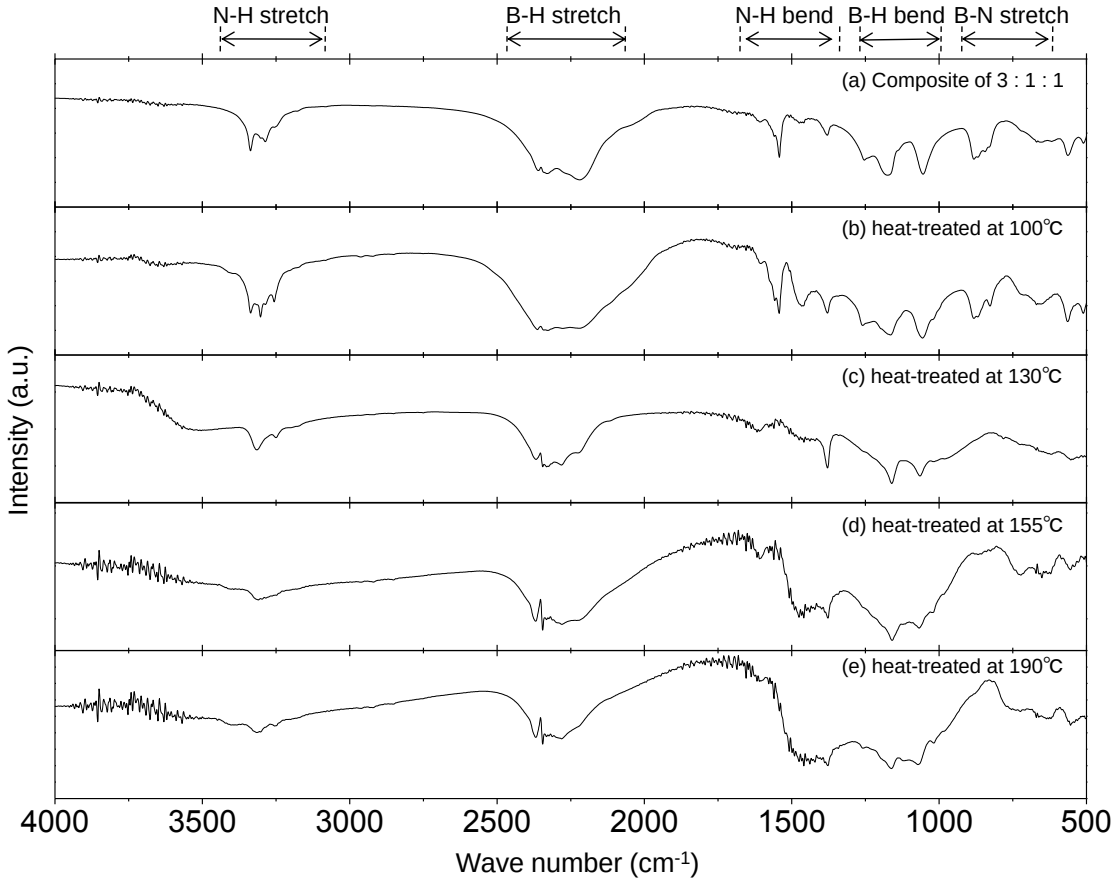

Figure 3-5 FTIR spectra of (a) Composite of NH_3BH_3 : MgH_2 : $NaNH_2$ = 3 : 1 : 1 at R.T., (b) heat-treated at 100 ºC, (c) heat-treated at 130 ºC, (d) heat-treated at 155 ºC, (e) heat-treated at 190 ºC

From the above results, it can be seen that AB and MgH_2 remained in the composite (NH_3BH_3 : MgH_2 : $NaNH_2$ = 3 : 1 : 1). If the single phase of $NaMg(NH_2BH_3)_3$ is formed in the composite, the synthesis reaction formula could be written as follows:

$$3NH_3BH_3 + MgH_2 + NaNH_2 \rightarrow NaMg(NH_2BH_3)_3 + NH_3 + 2H_2 \quad (3\text{-}2)$$

However, the XRD patterns of heat-treated samples contained MgH_2 and the results of NMR and FRIR contained AB. Therefore, actually the following reaction would occur in the composite as below.

$$3NH_3BH_3 + MgH_2 + NaNH_2$$

$$\rightarrow 1/2Na_2Mg(NH_2BH_3)_4 + NH_3BH_3 + 1/2MgH_2 + NH_3 + H_2 \quad (3\text{-}3)$$

When NH_3BH_3, MgH_2 and $NaNH_2$ are milled in a molar ratio of 3 : 1 : 1, solid phases of NH_3BH_3 and MgH_2 would remain except $Na_2Mg(NH_2BH_3)_4$. Thus, the XRD results of Fig. 3-3 are well consistent with the explanation based on equation (3-3) because unreacted MgH_2 is always observed in the XRD patterns. Also, unknown phases could be NH_3BH_3 or its related compound (*e.g.* ammonia absorption phase at 100 ºC).

3.3.2 Decomposition process of the composite (NH_3BH_3:MgH_2:$NaNH_2$=4:1:2)

In order to prepare $Na_2Mg(NH_2BH_3)_4$, the compound of NH_3BH_3, MgH_2 and $NaNH_2$ were mixed at a molar ratio of 4 : 1 : 2 and processed by ball-milling for 12 hours. Figure 3-6 shows the results of thermal analysis on $Na_2Mg(NH_2BH_3)_4$. Total weight loss was 13 wt.% due to the gas emission of hydrogen and ammonia as shown in the result of MS. In the results of DTA, two endothermic reactions were confirmed. Ammonia of about 5 wt.% was released in the first reaction. This means that 0.6 mol of ammonia is absorbed in 1mol of $Na_2Mg(NH_2BH_3)_4$ according to the results of ammonia PCI measurement in chapter 4. Hydrogen gas of 7.5 wt.% was released in the second reaction with endothermic. The range of hydrogen release temperature was well consistent with the previous report of $Na_2Mg(NH_2BH_3)_4$. [1, 2]

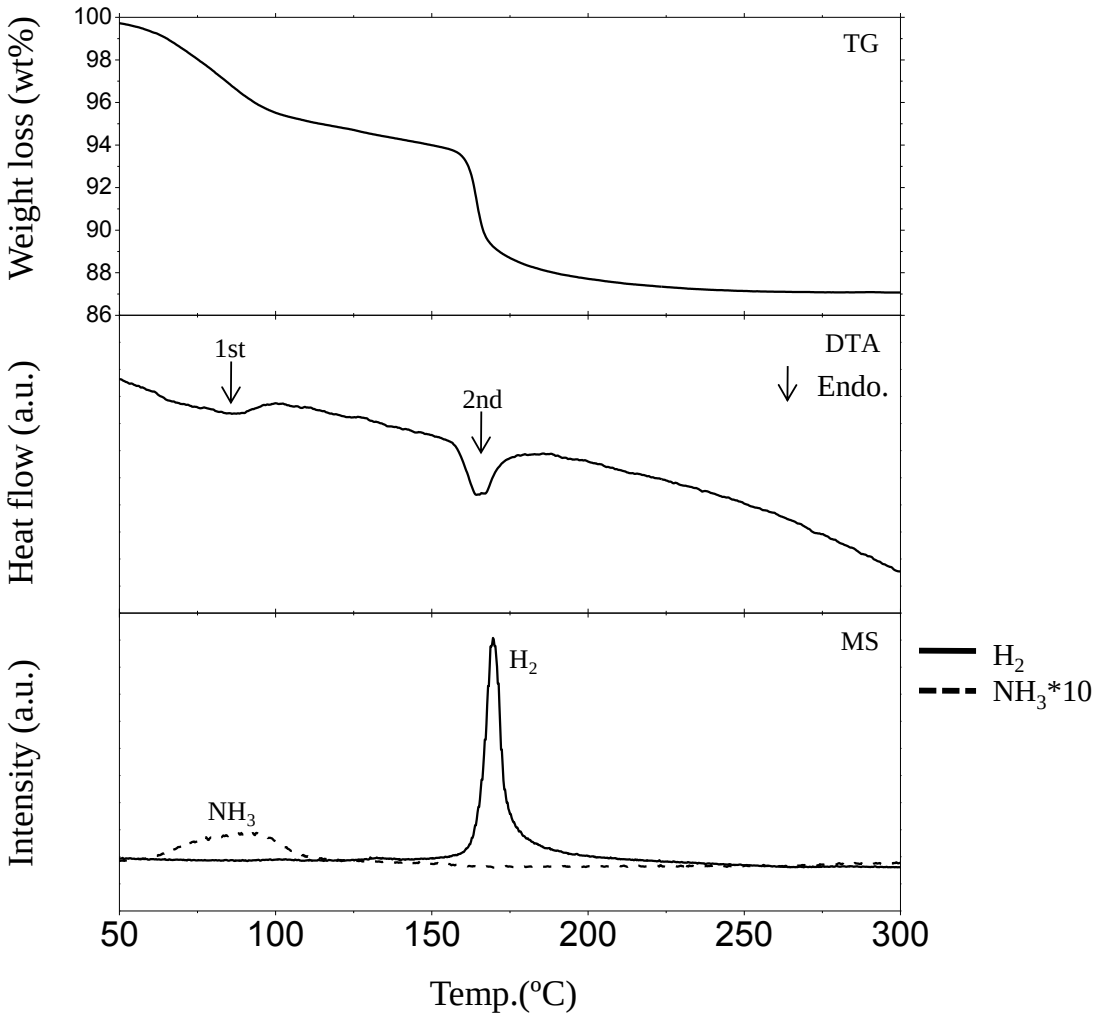

Fig.3-6 TG/DTA/MS profiles of Composite (NH_3BH_3 : MgH_2 : $NaNH_2$ = 4 : 1: 2)., MS (Solid line : hydrogen, dashed line : ammonia*10), heating rate = 5ºC /min, He flow

Figure 3-7 shows the results of XRD for samples of ball-milled and heat-treated at 100 ºC and 300 ºC. Compared with previous studies, main peaks were $Na_2Mg(NH_2BH_3)_4$ and some peaks of unknown phase existed in Fig. 3-7 (a). [1, 2] In the result of Fig. 3-7 (b) (after the end of first reaction), unknown phases disappeared and only the peaks of $Na_2Mg(NH_2BH_3)_4$ were present. Since the first reaction releases only ammonia gas up to 120 ºC, the unknown phase present in Fig. 3-7 (a) would be ammonia absorbed Na-Mg amidoborane ($Na_2Mg(NH_2BH_3)_4 \cdot nNH_3$). It is thought that the ammonia gas is generated during the synthesis of $Na_2Mg(NH_2BH_3)_4$ as shown in the following equation (1).

$$4\ NH_3BH_3 + MgH_2 + 2\ NaNH_2 \rightarrow Na_2Mg(NH_2BH_3)_4 + 2\ NH_3 + 2\ H_2$$

$$\rightarrow (1\text{-}x)\ Na_2Mg(NH_2BH_3)_4 + x\ Na_2Mg(NH_2BH_3)_4 \cdot nNH_3 + 2\ H_2 \quad (1)$$

After heating up to 300 ºC, the peaks of $Na_2Mg(NH_2BH_3)_4$ disappeared as shown in Fig. 3-7 (c). A broad peak between 40º and 50º was amorphous phase, which would originate from the decomposition product of $Na_2Mg(NH_2BH_3)_4$. Broad peaks around 20º and 30º originate from the polyimide film and grease to prevent the sample oxidation.

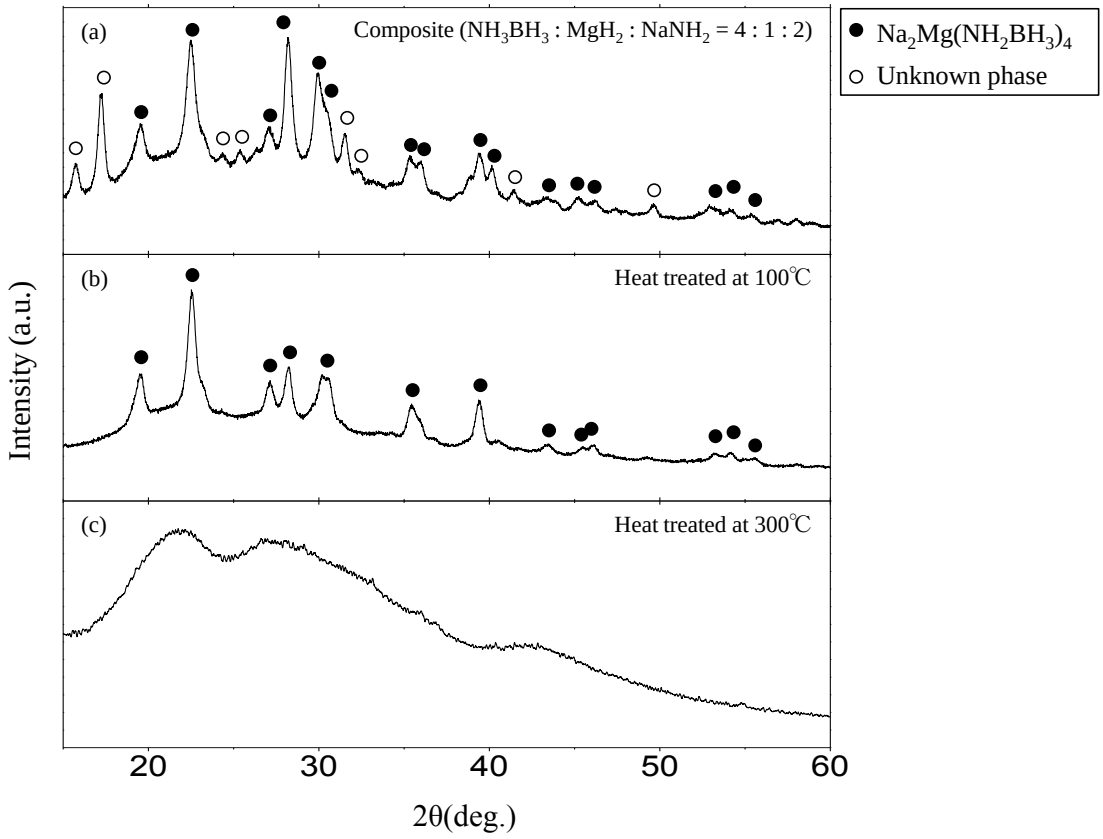

Fig.3-7 XRD patterns of (a) composite (NH_3BH_3 : MgH_2 : $NaNH_2$ = 4 : 1: 2) at R.T., (b) heat-treated at 100 ºC, (c) heat-treated at 300 ºC

As the summary of above results, the composite (NH_3BH_3 : MgH_2 : $NaNH_2$ = 3 : 1 : 1) showed the different decomposition process compared with the composite (NH_3BH_3 : MgH_2 : $NaNH_2$ = 4 : 1 : 2). The single endothermic hydrogen release reaction of the composite (4 : 1 : 2) would originate from the decomposition of $Na_2Mg(NH_2BH_3)_4$. After the desorption, only amorphous phase was observed in the XRD profile. However, in the composite (3 : 1 : 1), four hydrogen desorption steps were observed. In the XRD profiles, MgH_2 and unknown phase were observed during the decomposition process. Since the crystal structure of $NaMg(NH_2BH_3)_3$ was not analyzed and the XRD profile of $NaMg(NH_2BH_3)_3$ was quite similar to $Na_2Mg(NH_2BH_3)_4$, we propose that

$Na_2Mg(NH_2BH_3)_4$ would preferentially formed in the composite (3 : 1 : 1). If the $Na_2Mg(NH_2BH_3)_4$ is formed, MgH_2, NH_3BH_3, NH_3, and H_2 would remain. This is consistent with the XRD results in Fig. 6. Thus, we suggest that endothermic hydrogen release would originate from $Na_2Mg(NH_2BH_3)_4$ and exothermic ones would originate from the reaction among $Na_2Mg(NH_2BH_3)_4$ and the remaining products in the composite (3 : 1 : 1).

3.4 Summary

In this chapter, a study on dehydrogenation processes of Na-Mg amidoborane ($NaMg(NH_2BH_3)_3$ and $Na_2Mg(NH_2BH_3)_4$) was performed with the same starting materials and milling condition. The product of each sample was analyzed using XRD, NMR, FTIR. The thermal decomposition characteristics of the samples were analyzed by TG-DTA-MS. The results showed that $Na_2Mg(NH_2BH_3)_4$ were synthesized by ball-milling with a new combination of NH_3BH_3, MgH_2 and $NaNH_2$. In the result of molar ratio 3 : 1 : 1, $Na_2Mg(NH_2BH_3)_4$ also preferentially formed. Thus, the endothermic dehydrogenation from Na-Mg amidoborane would originate from $Na_2Mg(NH_2BH_3)_4$ phase. Also, we found the $Na_2Mg(NH_2BH_3)_4$ absorbed ammonia gas to form ammonia absorbed Na-Mg amidoborane.

References

1. H. Wu *et al*., Sodium magnesium amidoborane: the first mixed-metal amidoborane, *Chem. Commun.,* 47 (2011) 4102 - 4104
2. Y. S. Chua *et al*., From Exothermic to Endothermic Dehydrogenation-Interaction of Monoammoniate of Magnesium Amidoborane and Metal Hydrides, *Chem. Mater.*, 24 (2012) 3574 - 35812
3. X. Kang *et al*., Combined formation and decomposition of dual-metal amidoborane $NaMg(NH_2BH_3)_3$ for high-performance hydrogen storage, *Dalton Trans,* 40 (2011) 3799
4. K. Shimoda *et al*., Solid state NMR study on the thermal decomposition pathway of sodium amidoborane NaNH2BH3, *J. Mater. Chem.*, 21 (2011) 2609
5. C. Gervais *et al*., High resolution solid state NMR investigation of various boron nitride preceramic polymers, *Journal of Organometallic Chemistry,* 657 (2002) 75-82
6. G. Guella *et al*., New Insights on the Mechanism of Palladium-Catalyzed Hydrolysis of Sodium Borohydride from ^{11}B NMR Measurements, *J. Phys. Chem. B 110 (*2006) 17024-17033
7. S.M. Lee *et al*., A Comparative Study of the Structural, Electronic, and Vibrational Properties of NH_3BH_3 and $LiNH_2BH_3$: Theory and Experiment, *ChemPhysChem*, 10 (2009) 1825-1833

Chapter 4

Re-hydrogenation of $Na_2Mg(NH_2BH_3)_4$

4.1 Background and purpose

As indicated in chapter 1, the possibility of re-hydrogenation of hydrogen storage materials is very important. The metal hydrides that can be easily re-hydrogenated have extremely low hydrogen storage capacity compared to the target value of NEDO (7.5 mass %). [1] There are several reports of hydrogen storage materials that can be re-hydrogenated while meeting the DOE targets. [2-5] Among them, aluminum hydride (AlH_3) re-hydrogenated at 8.9 GPa and 600 °C and recovery of AlH_3 at ambient conditions. [2-3] However, because the required hydrogen pressure is very high, it is not suitable for practical use.

In ammonia borane system, there has been no successful re-hydrogenation. However, there are some reports that the enthalpy change of dehydrogenation becomes endothermic. [6-10] As shown Fig. 4-1, The first endothermic reaction (39 kJ/mol) corresponds to the melting/decomposition of β-$Al(BH_4)_3 \cdot NH_3BH_3$. The next endothermic reaction (65 kJ/mol) is assigned to the second decomposition step. [6] However, $Al(BH_4)_3 \cdot NH_3BH_3$ could not be re-hydrogenated despite having the endothermic reaction. In the result of $Na_2Mg(NH_2BH_3)_4$, it was observed that hydrogen was released by endothermic reaction (5.2 kJ/mol) at around 158 °C. [10] However, re-hydrogenation experiments have not been conducted. Therefore, the purpose of this chapter is to investigate the re-hydrogenability of $Na_2Mg(NH_2BH_3)_4$ using high pressure hydrogen gas equipment.

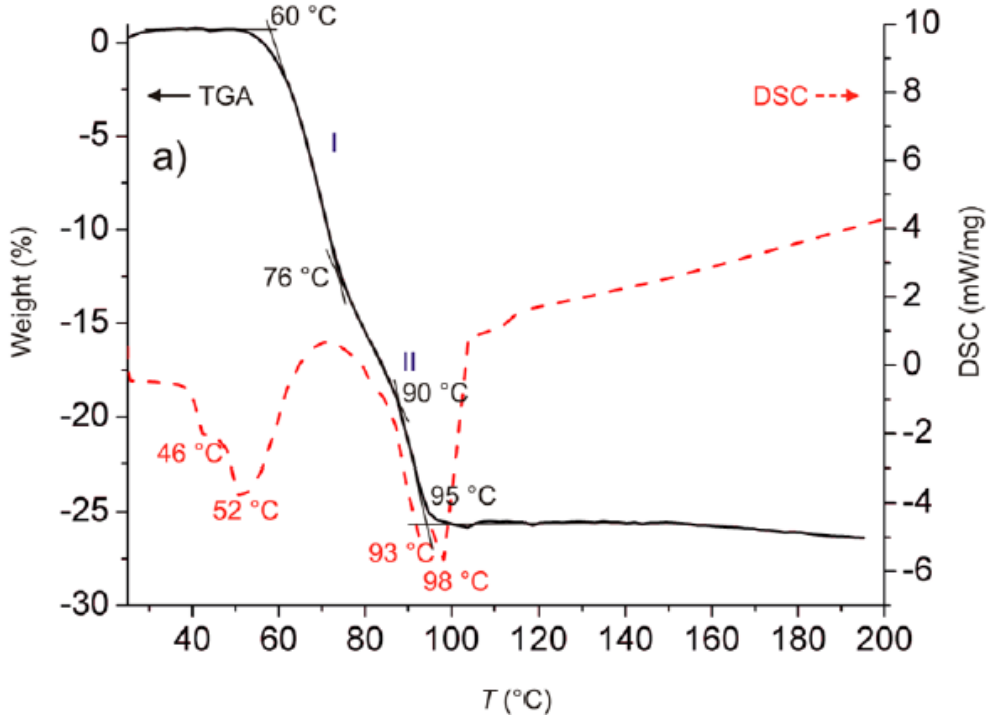

Fig. 4-1 The TGA and DSC data of $Al(BH_4)_3 \cdot NH_3BH_3$ complex (a rate of 1 °C/min)

4.2 Experimental procedure

4.2.1 Sample synthesis

NH_3BH_3 (Sigma-Aldrich, purity 97%), MgH_2 (Alfa Aesar, purity 98%), and $NaNH_2$ (Sigma-Aldrich, purity 98%) were weighed to be totally 300 mg, and mixed at molar ratios of NH_3BH_3 : MgH_2 : $NaNH_2$ = 4 : 1 : 2 by using planetary ball-mill apparatus (Fritsch Pulverisette 7). The milling was performed using steel balls of total 21 g under 1.0 MPa of H_2 atmosphere, at 400 rpm for 12 hours, with 30 min operation and 15 min interval. All sample handlings were performed in a glove box with Ar atmosphere. In order to clarify re-hydrogenation, decomposed $Na_2Mg(NH_2BH_3)_4$ was prepared by heat treatment. Heat treatment conditions are carried out at a heating rate 5 ºC/min from room temperature to 190 ºC, and then maintained at 190 ºC for 1 hour.

4.2.2 Re-hydrogenation

High-pressure and high-temperature experiments were carried out using a cubic-anvil-type high-pressure apparatus at Spring-8. Figure 4-2 shows the schematics of the high-pressure cell assemblies with hydrogen sources. [4] A high-pressure cell used in the present study consisted of a cubic pressure-transmitting medium, a resistant heater, a hydrogen-sealing capsule, internal hydrogen source which decomposed at around 550 ºC to immerse sample in hydrogen. The powder samples were filled in pyrolytic boron nitride (PBN) capsules. Then, place hydrogen sources ($NaBH_4$ + $Ca(OH)_2$) above and below PBN capsule and wrap in NaCl capsules and graphite heater and pyrophyllite.

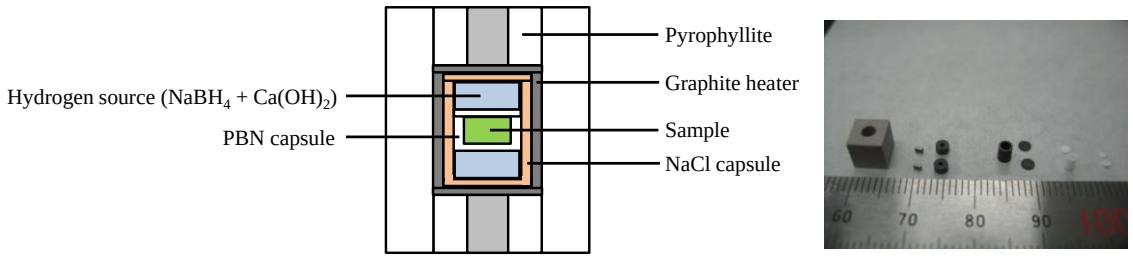

Fig. 4-2 The schematics of the high-pressure cell and real size photograph

The re-hydrogenation reactions were carried out as Fig. 4-3. All samples were pressurized to ~9 GPa for 2 hours at room temperature (R.T.). Then, the sample and hydrogen sources were heated to 550 ºC at a rate of 100 ºC/min to evolve hydrogen. Sample 1 was immediately cooled to 300 ºC for 1 min. Thereafter, the temperature was maintained at 300 ºC for 2 hours and then cooled to R.T. And sample 2 was immediately cooled to 300 ºC for 1 min. Thereafter, the temperature was cooled over 12 hours from 300 ºC to R.T. Finally, sample 3 was immediately cooled to 150 ºC for 1 min. Then, the temperature was maintained at 150 ºC for 24 hours and then cooled to R.T.

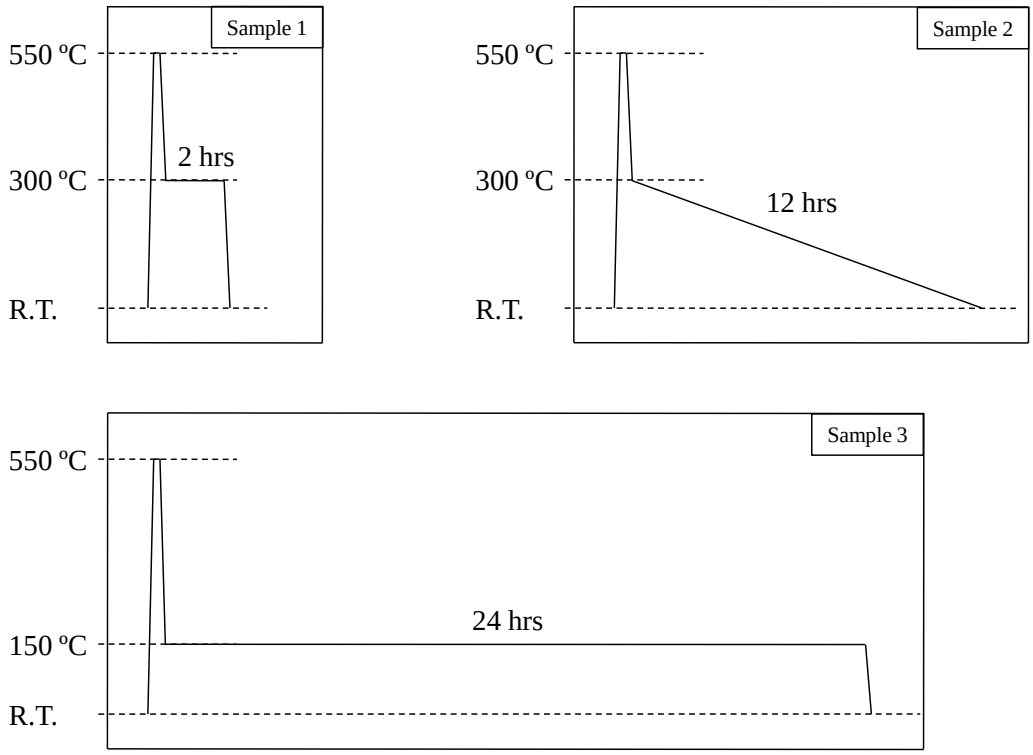

Fig. 4-3 Re-hydrogenation temperature condition of samples

4.2.3 Characterization

The crystalline phases were identified by angle-dispersive X-ray diffraction (ADX). [4] The energy dispersive X-ray diffraction (EDX) method allows acquisition of diffraction data from a very limited reciprocal lattice space. The outputs of the filament voltage and current were 40 kV and 100 mA, respectively. The sample was set on a glass plate and covered with a polyimide sheet (Kapton tape) in glove box for avoiding the samples exposed to the air. The detection of the hydrogen emission peaks was measured using a direct coupled mass spectrometer (MS, ULVAC, BGM-102). The direct coupled mass spectrometer is an apparatus in which the distance between the sample reaction unit and the MS measurement unit is shortened in order to detect a small amount of emitted gas from the sample. By using this device, it was possible to detect a hydrogen emission peak even with a sample amount of 0.1 mg which cannot be detected by ordinary TG-DTA-MS.

4.3 Results and discussions

4.3.1 Phase identification of samples

In order to confirm the re-hydrogenation, phase identification was performed by ADX. Each result is one-dimensionalized of X-ray diffraction image and the value was converted to the result of powder XRD with Cu Kα radiation. Fig. 4-4 a) is the result after heating $Na_2Mg(NH_2BH_3)_4$ to 550 ºC at a pressure of 9 GPa. Fig. 4-4 b) - d) show the results after re-hydrogenation at each temperature condition. Finally, Fig. 4-4 e) shows the results after heating sample 3 to 200 ºC with TG-DTA-MS. A broad peak was observed around 10 degrees in all samples. From the results of Fig. 4-4 b), c) and d) under the respective temperature conditions, peaks of unknown phase were observed at 20 degrees and around 30 degrees. These peaks were not consistent with the initial material $Na_2Mg(NH_2BH_3)_4$, and was not consistent with other expected compounds. It was found that it became a new compound by re-hydrogenation. Also, it is considered that sample 3 has better crystallinity of the product than sample 1 and 2 from the intensity and sharpness of the peaks. Alternatively, the amount of product is considered to be high. The reason for setting different temperature conditions is that the activation energy and the hydrogen pressure for producing hydrides are important for re-hydrogenation. When the re-hydrogenation temperature is high, high pressure hydrogen is required. On the other hand, it was thought that the hydride could easily be produced to satisfy the activation energy. However, new products were formed by re-hydrogenation even at 150 ºC. After dehydrogenation, the peaks became sharper and the broad peaks around 30 degree became weaker in intensity. This is different from the results of XRD after decomposition of $Na_2Mg(NH_2BH_3)_4$ shown in chapter 3. In other words, high-pressure experiments suggest that a new phase has been created.

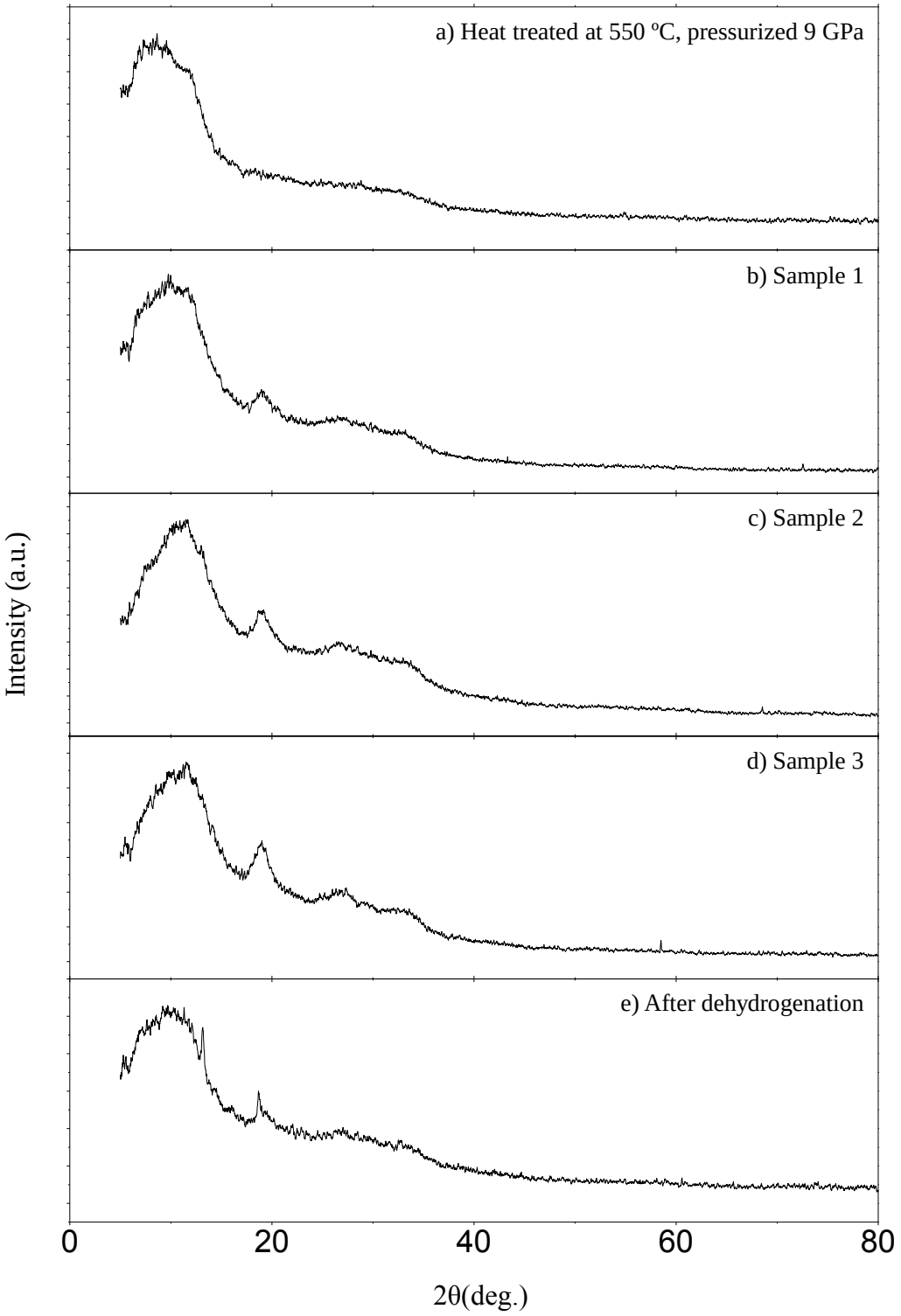

Fig. 4-4 XRD patterns of a) Heat treatment of $Na_2Mg(NH_2BH_3)_4$ at 550 ºC under 9 GPa., b) Sample 1, c) Sample 2, d) Sample 3, e) After dehydrogenation of sample 3

4.3.2 Dehydrogenation properties of re-hydrogenated sample

After re-hydrogenation, direct coupled MS experiments were performed to confirm that the sample had absorbed hydrogen. The amount of sample obtained from high-pressure re-hydrogenation experiments was a very small amount less than 0.1 mg. Therefore, the dehydrogenation reaction could not be detected by the usual TG-DTA-MS method for the following reasons; the distance between the reaction part of the sample and the measurement part of MS is long, using He gas to transport gas from TG-DTA to MS equipment. So, the dehydrogenation reaction was confirmed by using direct coupling type MS equipment. First, baking was performed at 300 ºC for 24 hours while vacuuming in order to remove impurities attached in the holder. After that, a sample of 0.1 mg or less was set in the glove box. And then, the holder was connected to the MS apparatus and vacuuming was performed for 30 minutes. Figure 4-5 a) shows MS result of hydrogen release when heated from R.T. to 300 ºC for 30 minutes. The heating rate could not be adjusted because of the setting of heating device. There were four peaks at 100 ºC, 168 ºC, 248 ºC and around 300 ºC which were considered to be hydrogen release, respectively. Figure 4-5 b) shows the result of MS when the dehydrogenated holder containing sample 3 was cooled to R.T. and then heated again to 300 ºC. As shown Fig. 4-5 b), the hydrogen emission peaks which was in a) disappeared. However, the release of hydrogen which did not decompose was detected at around 300 ºC.

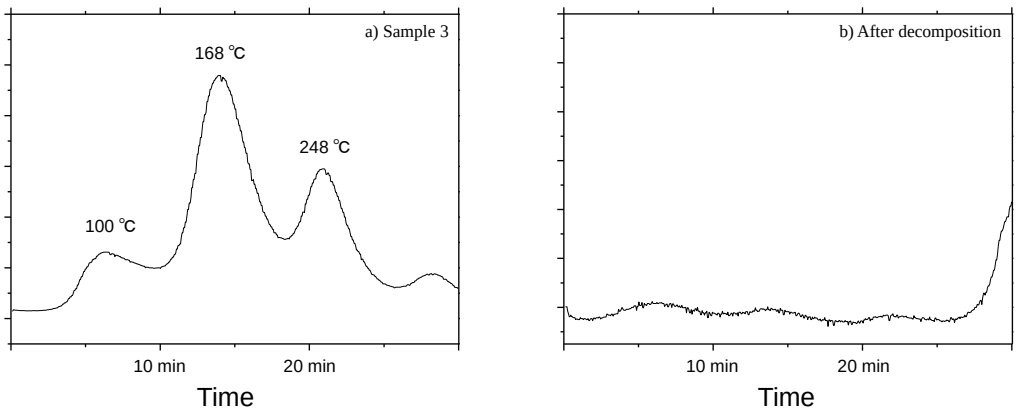

Fig. 4-5 Direct coupled mass spectrometer (MS) results of a) sample 3, b) after decomposion

4.4 Summary

In this chapter, a study on re-hydrogenation of $Na_2Mg(NH_2BH_3)_4$ was performed using high-pressure hydrogen gas equipment. The unidentified solid phase was confirmed from the results of ADX. According to direct coupling MS measurement, this phase released hydrogen in several steps by raising the temperature. Therefore, The decomposed $Na_2Mg(NH_2BH_3)4$ was converted to an unknown phase under high pressure hydrogen and can store hydrogen.

Reference

1. https://www.nedo.go.jpcontent100642946.pdf
2. H. Saitoh *et al*., Formation and decomposition of AlH_3 in the aluminum-hydrogen system, *Appl. Phys. Lett.*, 93 (2008) 151918
3. H. Saitoh *et al*., Hydrogenation of passivated aluminum with hydrogen fluid, *Appl. Phys. Lett.*, 94 (2009) 151915
4. H. Saitoh *et al*., Formation and crystal growth process of AlH_3 in Al–H system, *Journal of Alloys and Compounds*, 496 (2010) L25-L28
5. G. Liang *et al*., Hydrogen storage properties of the mechanically milled MgH_2-V nanocomposite, *Journal of Alloys and Compounds*, 291 (1999) 295–299
6. I. Dovgaliuk *et al*., Mild Dehydrogenation of Ammonia Borane Complexed with Aluminum Borohydride, *Chem. Mater.*, 27 (2015) 768−777
7. Anna V. Pomogaeva *et al*., Mechanisms of Hydrogen Generation from Tetrameric Clusters of Lithium Amidoborane, *J. Phys. Chem. A*, 120 (2016) 145−152
8. X. Kang *et al*., Combined formation and decomposition of dual-metal amidoborane $NaMg(NH_2BH_3)_3$ for high-performance hydrogen storage, *Dalton Trans.*, 40 (2011) 3799
9. H. Wu *et al*., Sodium magnesium amidoborane: the first mixed-metal amidoborane, *Chem. Commun.*, 47 (2011) 4102-4104
10. Y. S. Chua *et al*., From Exothermic to Endothermic Dehydrogenation - Interaction of Monoammoniate of Magnesium Amidoborane and Metal Hydrides, *Chem. Mater.*, 24 (2012) 3574−3581
11. H. Wu *et al*., A new family of metal borohydride ammonia borane complexes: Synthesis, structures, and hydrogen storage properties, *J. Mater. Chem.*, 20 (2010) 6550–6556

Chapter 5

Ammonia ab/desorption of $Na_2Mg(NH_2BH_3)_4$

5.1 Background and purpose

In many reasons, ammonia has been already considered a perfect hydrogen carrier. [1] For that reasons, it is produced at essentially the same cost as hydrogen. Secondly, it can be used available in larger quantities than any other pure chemical. Finally, it is distributed through existing global infrastructure. An additional important property of ammonia is that it can be decomposed into hydrogen and nitrogen. [2, 3] For this reason, the studies on materials that absorb and release ammonia have been carried out steadily. Some halides and complex hydrides can absorb a large amount of ammonia, thus these materials are promising for decreasing ammonia vapor pressure effectively and safely. [4, 5] The reactions to form the ammine complexes after the NH3 absorption into metal halides and metal borohydrides are shown in the following equations 5-1 and 5-2, respectively.

$$MX_m + nNH_3 \leftrightarrows M(NH_3)_nX_m \qquad (5\text{-}1)$$

$$M(BH_4)_m + nNH_3 \leftrightarrows M(NH_3)_n(BH{=})_m \qquad (5\text{-}2)$$

In the case of N-B-H system, NH_3BH_3 absorbed 6 equiv of NH_3 under 1-4 bar ammonia gas at 0 ºC.[6] Also, $Mg(NH_2BH_3)_2$ and $Al(NH_2BH_3)_3$ can form the ammoniates as new crystalline phases.[7, 8] However, study on ammonia absorption of Na-Mg amidoborane has not been conducted yet.

In this work, we found a new ammonia absorption phase of $Na_2Mg(NH_2BH_3)_4$ by using $NaNH_2$ as a starting material. We investigated the ammonia absorption properties of Na-Mg amidoborane by pressure-composition isothermal measurement. This is the first experimental description of the ammonia absorption properties of $Na_2Mg(NH_2BH_3)_4$.

5.2 Experimental procedure

5.2.1 Sample synthesis

NH_3BH_3 (Sigma-Aldrich, purity 97%), MgH_2 (Alfa Aesar, purity 98%), and $NaNH_2$ (Sigma-Aldrich, purity 98%) were weighed to be totally 300 mg, and mixed at molar ratios of NH_3BH_3 : MgH_2 : $NaNH_2$ = 4 : 1 : 2 by using planetary ball-mill apparatus (Fritsch Pulverisette 7). The milling was performed using steel balls of total 21 g under 1.0 MPa of H_2 atmosphere, at 400 rpm for 12 hours, with 30 min operation and 15 min interval. All sample handlings were performed in a glove box with Ar atmosphere. In order to clarify the absorption of ammonia gas, $Na_2Mg(NH_2BH_3)_4$ which ammonia was released was prepared by heat treatment. Heat treatment conditions are carried out at a heating rate 5 ºC/min from room temperature to 100 ºC, and then maintained at 100 ºC for 1 hour.

5.2.2 Characterization

The crystalline phases were identified by powder X-ray diffraction (XRD, RIGAKU RINT-2500 with Cu Kα radiation). The outputs of the filament voltage and current were 40 kV and 200 mA, respectively. The sample was set on a glass plate and covered with a polyimide sheet (Kapton, Du Pont-Toray Co. LTD) with grease (Apiezon, M&I material Ltd.) in glove box for avoiding the samples exposed to the air. The absorption behavior of $Na_2Mg(NH_2BH_3)_4$-NH_3 system was evaluated by using pressure-composition isothermal (PCI) measurement (BELSORP- HP-nex for ammonia gas).[4, 5] The features of the device are the ability to measure adsorption isotherms, sorption isotherms and adsorption rates at high pressure (up to 1.0 MPa). After being attached to a PCI device and vacuuming the sample tube at 20 ° C for 30 minutes, the ammonia adsorption measurement was started. NH_3 absorption properties were measured in the pressure range from 0 to 666 kPa at 20 ºC. The temperature was kept by thermoelectric cooler. When the pressure change for 900 seconds is within 1000 Pa, it is judged to be in an equilibrium state.

5.3 Results and discussions

5.3.1 Ammonia ab/desorption property of $Na_2Mg(NH_2BH_3)_4$

Ammonia gas PCI (pressure-composition isothermal) measurement was conducted to confirm whether the unknown phase in Chapter 3 was ammonia absorbed Na-Mg amidoborane or not. Figure 5-1 shows the PCI profiles of $Na_2Mg(NH_2BH_3)_4$ which was synthesized by the heat treatment of the composite (NH_3BH_3 : MgH_2 : $NaNH_2$ = 4 : 1: 2) at 100 ºC for 1 hour. The NH_3 pressure are plotted as a function of the amount of absorbed NH_3 for 1mol of $Na_2Mg(NH_2BH_3)_4$ (mol/mol). In the profile of ammonia absorption, the synthesized $Na_2Mg(NH_2BH_3)_4$ showed two plateau pressures of around 50 kPa and 100 kPa, and the amount of absorbed NH_3 was 5 mol. After plateau pressure, the NH_3 pressure was linearly increased with the amount of absorbed NH_3. In previous study [4 - 6], the same phenomenon was found in the solid NH_3BH_3 and solid $NaBH_4$ ammine complex. In General, if the material does not absorb NH_3, the equilibrium pressure increases vertically and reaches 0.8 MPa immediately. However, with increase in the NH_3 pressure, the plateau of the PCI shows the reaction to form an ammine complex phase, if the plateau area appears and absorption of NH_3 is confirmed. After this phase was generated, the NH_3 absorption was stopped and its pressure reaches 0.8 MPa immediately. However, in $Na_2Mg(NH_2BH_3)_4$ sample, linear graph was obtained after plateau pressure. A linear increase in the ammonia pressure means that the solid complex absorbs ammonia while liquefying. So, this means that solid $Na_2Mg(NH_2BH_3)_4 \cdot nNH_3$ could be changed to liquid phase at a pressure of 100 kPa or more. It was also possible to visually confirm the trace of sample liquefaction after the experiment. A total of 15 moles of ammonia could be absorbed up to 600 kPa in the liquid phase. Thus, a large amount of ammonia absorption of $Na_2Mg(NH_2BH_3)_4$ may pave the way for developing new ammonia absorption materials based on dual-metal amidoborane species. In the desorption profile, the results is almost similar to the absorption profile. However, the difference between the absorption amounts of 3 - 5 is probably due to the phase difference produced during absorption and desorption. There are two plateaus at absorption, so two phases could be created.

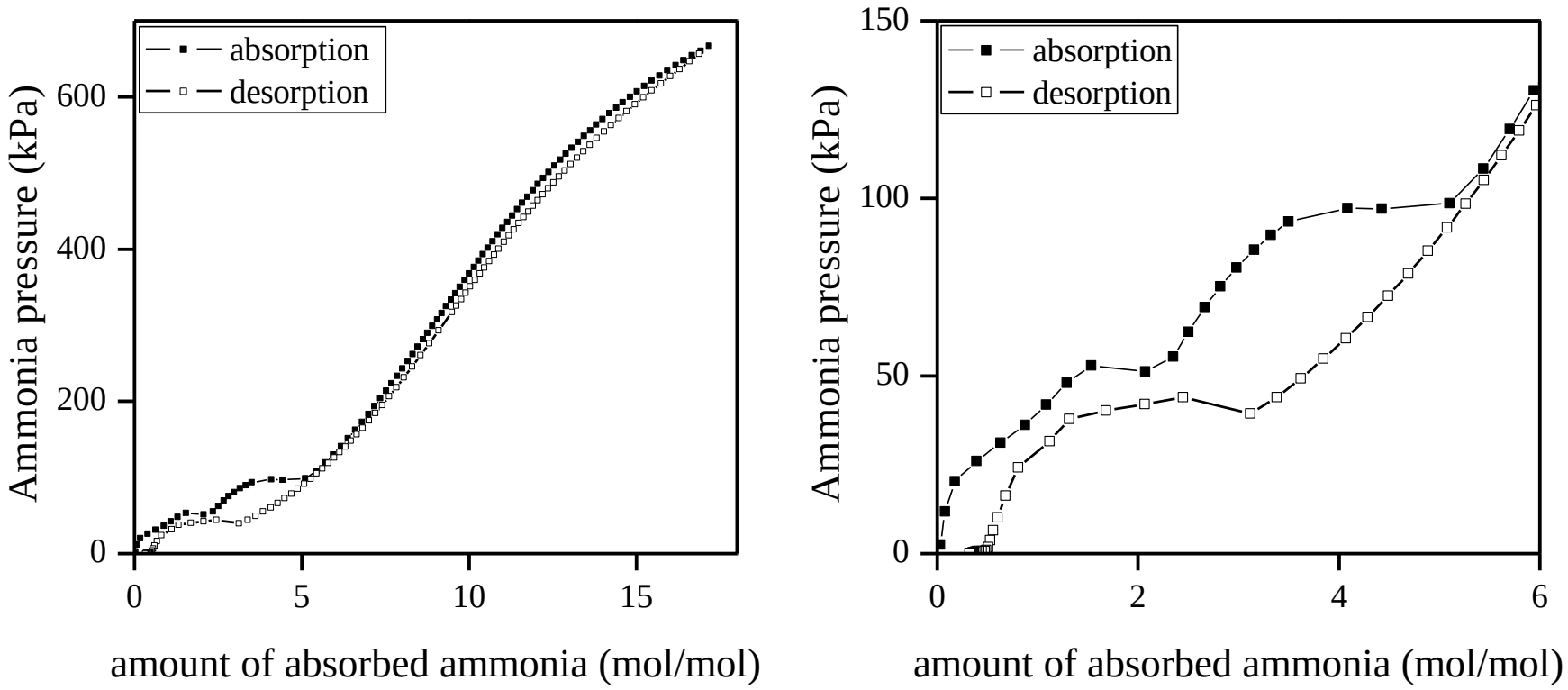

Fig. 5-1 Ammonia absorption and desorption curve for $Na_2Mg(NH_2BH_3)_4$ at 20ºC from 0 to 666 kPa,

On the other hand, since there is one plateaus at desorption, the ammonia absorption phase of the liquid changes into a single solid phase. Alternatively, there may be a problem with the PCI measurement temperature setting.

5.3.2 Phase identification of samples before/after PCI measurement

The XRD experiment was performed to investigate the presence of the same ammonia absorbed phase after ball-milling and after PCI measurement. After the PCI measurement, the sample cell was evacuated to remove ammonia gas and then the product was analyzed. Figure 5-2 shows the results of XRD for samples of ball-milled and heat-treated at 100 ºC for 1 hour and after PCI measurement. As shown in the results of Fig. 5-2, $Na_2Mg(NH_2BH_3)_4$ was observed both after the heat treatment and after ammonia absorption. However, the unknown phase that existed in Fig. 5-2 (a) disappeared after the heat treatment. And it appeared again after PCI measurement. As explained above, this means that the unknown phase is ammonia absorbed Na-Mg amidobarane. According to the desorption profile in Fig. 5-1, there is about 0.5 mol in $Na_2Mg(NH_2BH_3)_4$, even after ammonia released. The exact formula of this ammonia adsorption phase is difficult to specify. However, it seems that $Na_2Mg(NH_2BH_3)_4$ and $Na_2Mg(NH_2BH_3)_4 \cdot nNH_3$ are mixed. XRD experiments with ammonia pressurized conditions are needed to confirm more precise phase. For different peaks in Fig. 5-2 (a) and (c), there is the possibility of different ammonia absorbed phase or impurity phase (from initial material *e.g.* NH_3BH_3). The detailed crystal structure analysis of the unknown phase is currently in progress.

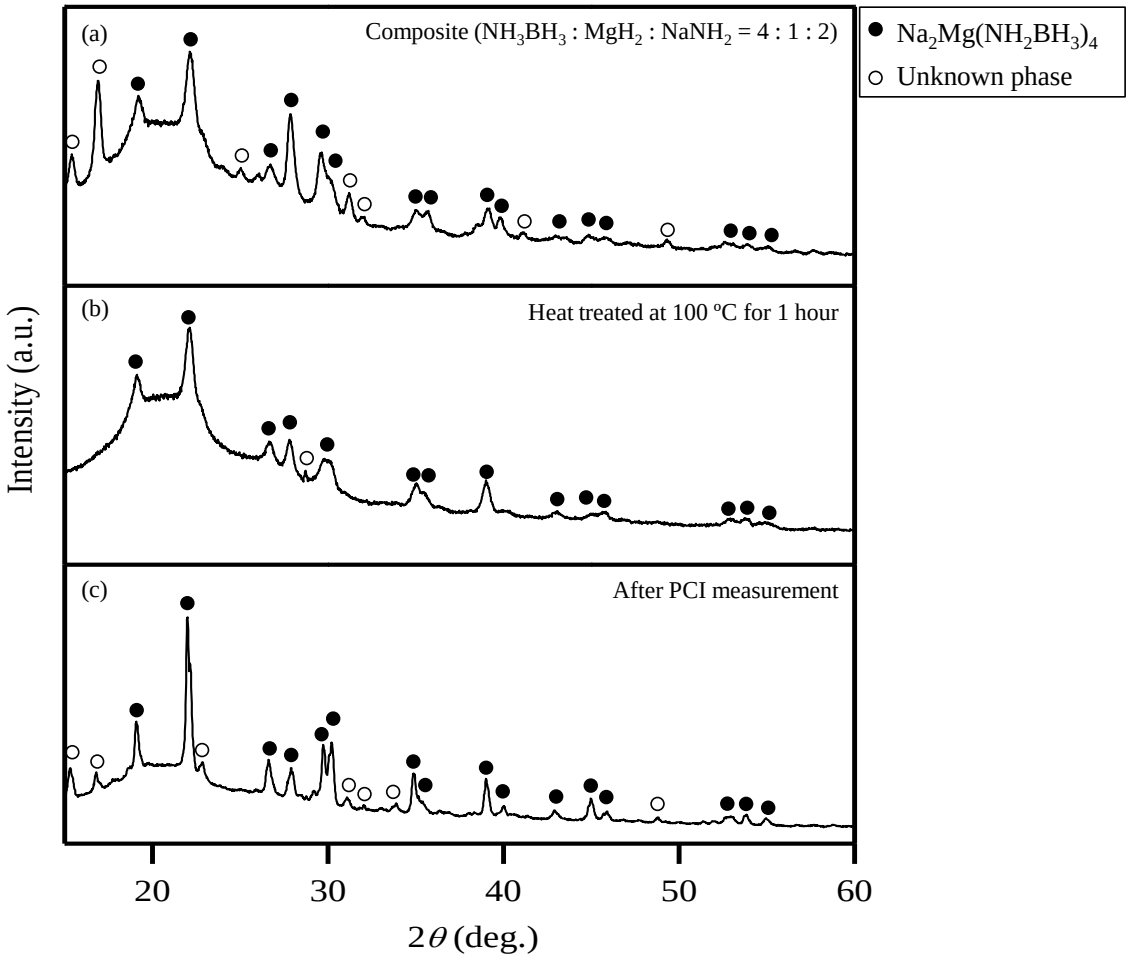

Fig. 5-2 XRD pattern of (a) composite (NH_3BH_3 : MgH_2 : $NaNH_2$ = 4 : 1: 2) (b) heat-treated at 100 ºC for 1 hour, (c) after PCI measurement

5.4 Summary

In this chapter, a study on ammonia absorption and desorption properties of $Na_2Mg(NH_2BH_3)_4$ was performed using PCI measurement and XRD. We found the $Na_2Mg(NH_2BH_3)_4$ absorbed ammonia gas to form ammonia absorbed Na-Mg amidoborane ($Na_2Mg(NH_2BH_3)_4 \cdot nNH_3$) as a new solid phase. According to PCI measurement, this phase further continued to absorb ammonia to form liquid phase. XRD experiments with ammonia pressurized conditions are required for the detailed crystal structure analysis.

Reference

1. Claus Hviid Christensen *et al*., Towards an ammonia-mediated hydrogen economy?, *Catalysis Today* 111 (2006) 140-144
2. T.V. Choudhary *et al*., Catalytic ammonia decomposition: COx-free hydrogen production for fuel cell applications, *Catalysis letter* 72 (2001) 197-201
3. Schlögl R *et al*., Catalytic synthesis of ammonia-a "never-ending story"?, *Angewandte chime* 42 (2003) 2004-2008
4. Taihei Aoki *et al*., Thermodynamics on Ammonia Absorption of Metal Halides and Borohydrides, *J. Phys. Chem* 118 (2014) 18412−18416
5. K. Nakajima *et al*., Operando spectroscopic analyses for the ammonia absorption process of sodium borohydride, *Chem.Comm.* 55 (2019) 2150-2153
6. L. Gao *et al*., Liquefaction of Solid-State BH3NH3 by Gaseous NH3 *Inorg. Chem.* 50 (2011) 4301-4306
7. X. Kang *et al*., A simple and efficient approach to synthesize amidoborane ammoniates case study for Mg(NH2BH3)2(NH3)3 with unusual coordination structure, *J. Mater. Chem.* 22 (2012) 13174-13179
8. J. Yang *et al*., Efficient Synthesis of an Aluminum Amidoborane Ammoniate, *Energies* 8, 9 (2015) 9107-9116,

Chapter 6
Hydrogen desorption properties of AlH_3

6.1 Background and purpose

As indicated in chapter 1, Although AlH_3 is the target of high capacity hydrogen storage materials of DOE, its poor reaction rate (kinetics) is a problem. Among the various methods to improve the problem, the addition of just 1 mol% NbF_5 remarkably destabilized γ-AlH_3 in the composite and led to its decomposition at room temperature. However, the effect of Nb-based additives on AlH_3 has not been reported. Therefore, the purpose of this chapter is to investigate Nb species doping effect on hydrogen release of AlH_3.

6.2 Experimental procedure

6.2.1 Sample synthesis

Commercially available Nb (Kojundo Chemical Lab., 99.99 %), Nb_2O_5 (Kojundo Chemical Lab., 99.99 %), NbF_5 (Sigma Aldrich, 98 %) and AlF_3 (Sigma Aldrich, 99.9 %) were used as-received for this research. AlH_3 was prepared by the chemical reaction between $LiAlH_4$ and $AlCl_3$ in ether solution. [1] The samples were prepared by ball-milling AlH_3 and Nb species using a planetary ball-mill apparatus (Fritsch Pulverisette 7) with 21 g of stainless balls and 100 mg samples. The milling was performed under 0.1 MPa Ar with 200 rpm for 1 h with two cycles of 30/15 min operation/interval per each cycle. All material handlings were conducted under in a glove box filled with purified Ar gas in order to avoid oxidation.

6.2.2 Characterization

Hydrogen desorption properties were examined by a thermogravimetry and differential thermal analysis equipment (TG-DTA, Bruker 2000SA) connected to a mass spectrometer (MS, ULVAC, BGM-102). The desorbed gases are carried from TG-DTA

equipment to MS through a capillary by flowing high purity He gas as a carrier gas. The flow rate of He gas was set to 300 mL min^{-1}. The samples were heated from room temperature to 200 °C with a heating rate of 5 °C min^{-1}. The crystalline phases of samples were analyzed by powder X-ray diffraction (XRD, PANalytical, X'Pert-Pro with Cu Kα radiation). The samples for XRD were placed on a glass plate in a glovebox and then covered with a polyimide sheet and sealed by grease in order to avoid the oxidation during the measurement. SEM-EDS measurements were performed to observe the distribution states of Nb species by using JIB-4600F/HKD, JEOL. The chemical bonding states of samples were studied by using X-ray Photoelectron Spectroscopy (XPS, Thermo Fisher Scientific, ESCALab 250Xi) with Al Kα radiation.

6.3 Results and discussion

Figure 6-1 shows the hydrogen desorption properties of as-synthesized, ball-milled, and Nb species 1 mol%-doped AlH_3. As shown in Fig. 6-1(a) and (b), the hydrogen desorption temperature was reduced after ball-milling and doping with Nb species. The enhancement in the ball-milled AlH_3 would originate from the formation of metallic Al particles on the hydride surface as shown in the Chapter 1. In fact, the mass loss of ball-milled AlH_3 (-9 mass %) was lower than that of as-synthesized AlH_3 (-10 mass %), suggesting the formation of metallic Al nuclei during ball-milling. It seemed that Nb- and Nb_2O_5-doped AlH_3 showed the improvements of the desorption kinetics compared with ball-milled one. Among all the samples, NbF_5-doped AlH_3 showed the lowest desorption temperature. It started to release hydrogen from 60 °C with a peak temperature at 122 °C (Fig.6-1(b)). However, the hydrogen mass loss of NbF_5-doped AlH_3 was only -6 mass%, which was the least value among all the samples. We also measured the sample with 5 mol% NbF_5 doping, but most of the hydrogen was released during ball-milling (The desorbed hydrogen amount during heating was only -1 mas s%.). Thus, doping a large amount of NbF_5 promoted the decomposition during milling.

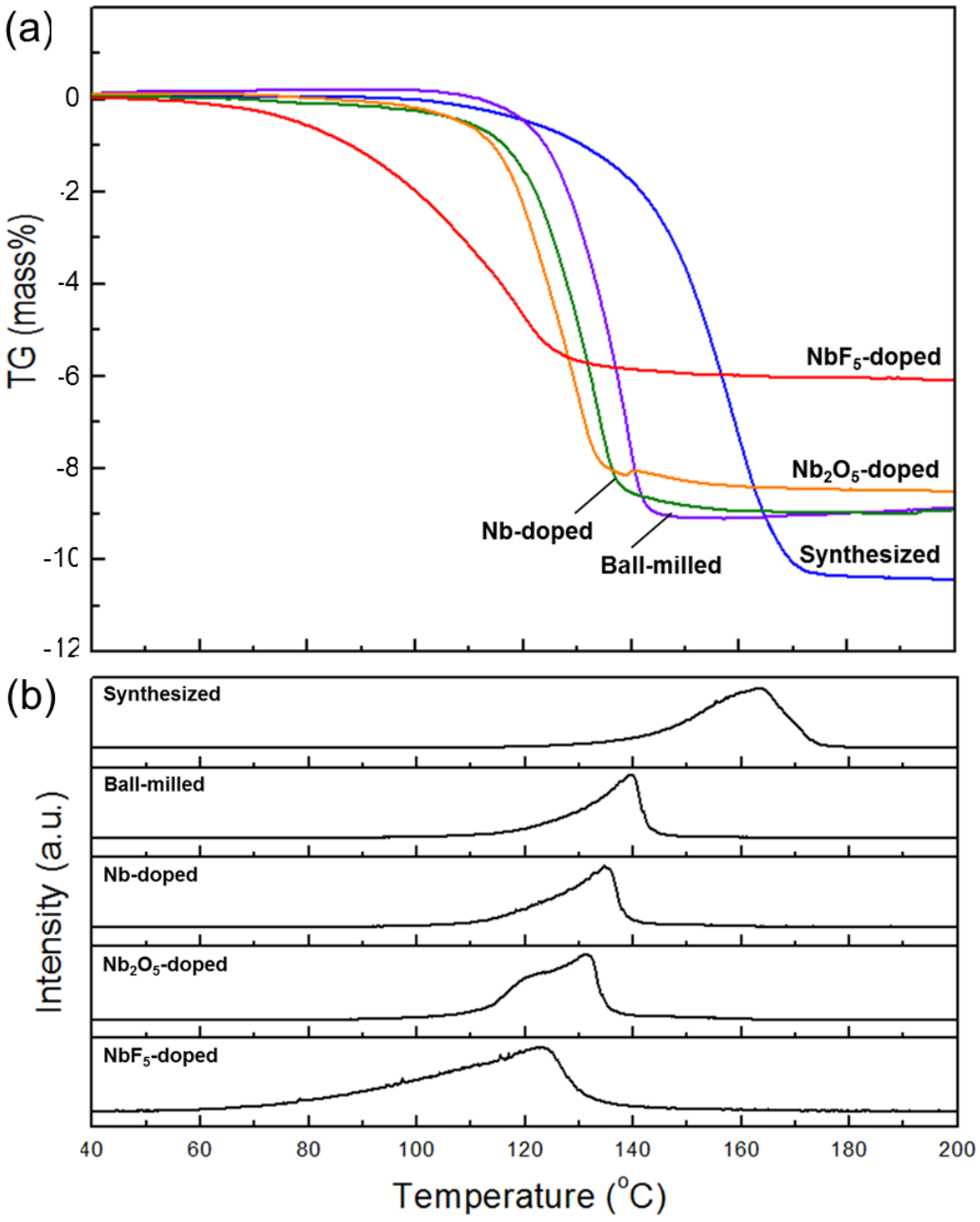

Fig.6- 1 (a) TG profiles and (b) MS (*m/z* = 2, H_2) profiles of as-synthesized, ball-milled, and Nb-, Nb_2O_5-, NbF_5-doped AlH_3. The amount of Nb species was 1 mol% in each doped sample. The heating rate was 5 °Cmin^{-1}. The weight loss value is based on the total system weight.

Figure 6-2 shows the XRD profiles of samples. Although as-synthesized sample contained α-AlH_3 and a small amount of γ-AlH_3, ball-milled one did not contain γ-AlH_3, probably due to its transformation to α-AlH_3 during milling. [2] The formation of NbH was observed in the Nb-doped AlH_3, indicating Nb reacted with AlH_3 during ball-milling. In the Nb_2O_5-doped AlH_3, Nb_2O_5 was observed after milling. In the case of Nb_2O_5-doped MgH_2 system, deoxidized Nb_2O_{5-x} phase was found on the surface of the samples. [3] Thus, the surface state of Nb_2O_5 could be also changed in the Nb_2O_5-doped AlH_3 system. On the other hand, Nb- or F-containing phases were not observed in any of the diffraction patterns of the NbF_5-doped AlH_3.

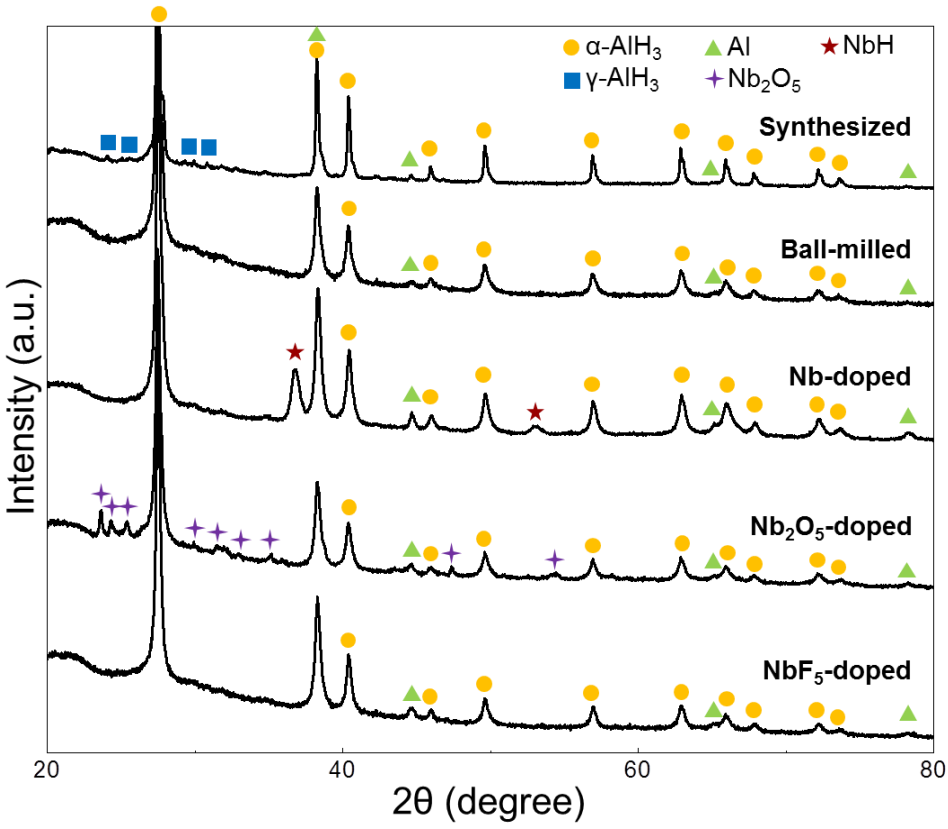

Fig.6-2 XRD patterns of as-synthesized, ball-milled, and Nb-, Nb_2O_5-, NbF_5-doped AlH_3. The amount of Nb species was 1 mol% in each doped sample

In order to investigate the distribution states of Nb dopants, SEM-EDS measurements were conducted for NbF_5- and Nb_2O_5-doped AlH_3 (Fig. 6-3). As shown in Fig. 6-3(a), micron-particles containing Nb or F were not detected from the EDS

analysis. Similar results were obtained in the case of 5 mol% NbF_5 doping. On the other hand, the micron-particles containing Nb and O were clearly observed in the Nb_2O_5-doped AlH_3. Thus, it seemed that Nb and F distributed uniformly on the surface of AlH_3 in the NbF_5-doped AlH_3. The fine distribution of Nb and F was also observed in other NbF_5-doped hydride systems. For instance, Kim *et al.* suggested that NbF_5 will melt during ball-milling and this promoted the presence of extremely fine Nb/NbH film on the surface of MgH_2 particles in NbF_5-doped MgH_2 system. [4, 5] Thus, compared with Nb- or Nb_2O_5-doped AlH_3, the fine distribution of dopant was achieved in the NbF_5-doped AlH_3.

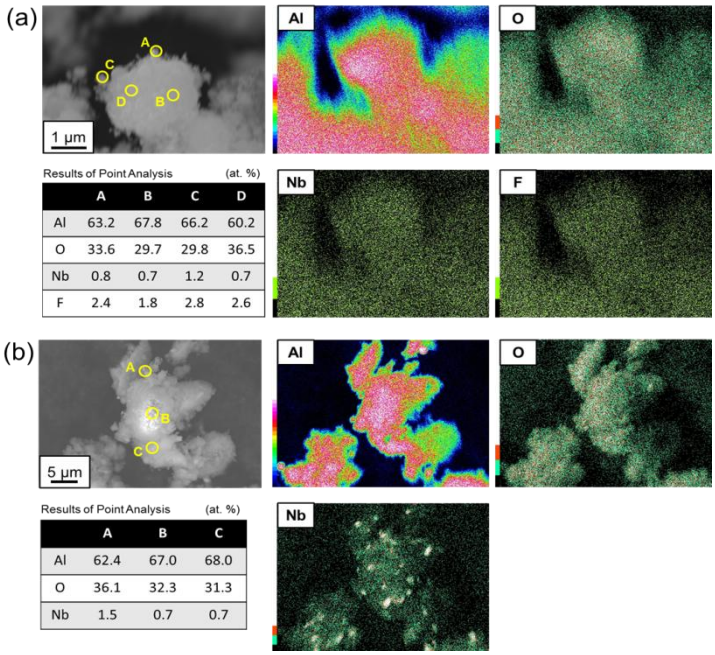

Fig.6-3 SEM-EDS results of (a) 1 mol% NbF_5-doped AlH_3 and (b) 1 mol% Nb_2O_5-doped AlH_3. Secondary-electron images and EDS results (point analysis and mapping images) are shown.

In order to get an insight on the desorption mechanism, further investigation was conducted for NbF_5-doped AlH_3, which showed the lowest onset temperature among all the samples. The activation energy for hydrogen desorption was analyzed for NbF_5-doped AlH_3. Figure 6-4 shows the Kissinger plot of the hydrogen desorption reaction for AlH_3 and NbF_5-doped AlH_3. The apparent activation energy for hydrogen desorption is calculated by using Kissinger equation [6],

$$\ln\frac{c}{T_p^2} = -\frac{E_a}{RT_p} + \ln\frac{RA}{E_a}$$

where E_a is the apparent activation energy for hydrogen desorption, c is the heating rate, T_p is the peak temperature, R is gas constant, and A is the frequency factor. The activation energies of hydrogen desorption for as-synthesized AlH_3, ball-milled AlH_3, and NbF_5-doped AlH_3 are calculated to be 111, 104, and 96 kJ/mol, respectively. The activation energies for as-synthesized and ball-milled AlH_3 were similar to the values in the previous study (104 kJ/mol, 102 kJ/mol [7]). The activation energy for NbF_5-doped AlH_3 was just slightly decreased compared with as-synthesized and ball-milled AlH_3. As shown in the Introduction part, Ti is known as an effective catalyst for AlH_3. It was reported that a decrease of the activation energy by at least 50 % is possible with the addition of Ti. [8] Thus, the effect of Nb on the decomposition kinetics would be less pronounced than that of Ti. The effect of cation species on the kinetics should be further clarified to understand the catalytic mechanism of AlH_3 system.

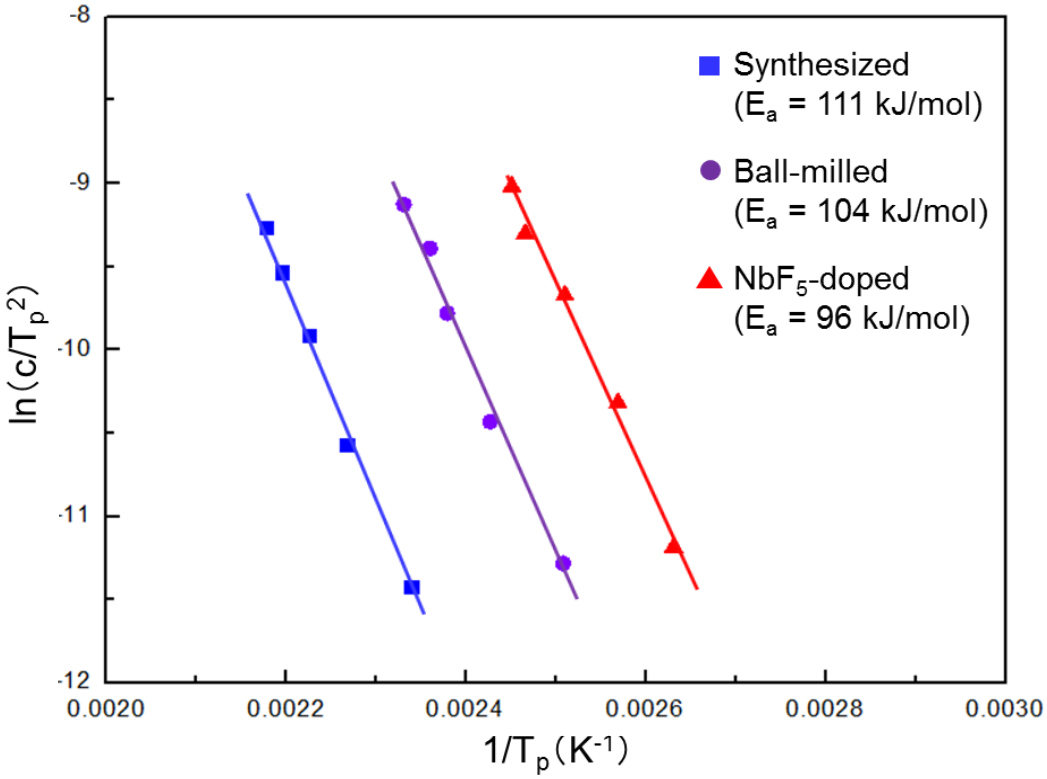

Fig.6-4 Kissinger plots for dehydrogenation of as-synthesized, ball-milled and 1 mol% NbF_5-doped AlH_3.

The bonding states of Nb and F elements were studied by using XPS. For comparison, the standard materials of NbF_5, Nb_2O_5 and AlF_3 were also measured. Figure 6-5 (a) shows the XPS spectra of Nb *3d* region. In the NbF_5-doped AlH_3, the binding energies of Nb $3d_{3/2}$ and $3d_{5/2}$ shift towards to the chemical states of Nb, suggesting the reaction between NbF_5 and AlH_3 would occur to form Nb. Also, shoulder peaks appeared between 204.0-212.0 eV, suggesting the presence of Nb oxide species *e.g.*, Nb_2O_5 and/or NbO. Figure 6-5 (b) shows the XPS spectra of F *1s* region. In the NbF_5-doped AlH_3, the binding energies of F *1s* peaks were observed at 686.5 eV (AlF_3) and a new peak at 684.8 eV. The new peak position is similar to the previously reported AlF_xO_y species [9], suggesting such kind of AlF_xO_y phase could exist. The broad peak at 688.9 eV in the starting material of AlF_3 might be attributed to the contamination of C-F species. [10] The XPS results suggest that the following reaction would occur during the milling process:

$$10\ AlH_3 + 6\ NbF_5 \rightarrow 10\ AlF_3 + 6\ Nb + 15\ H_2$$

whose Gibbs free energy $\Delta G° = -3570.4$ kJ [11,12] is possible from the thermodynamic potentials. The Nb spectrum in the NbF_5-doped AlH_3 (Fig.6-5 (a)) was similar to that of NbF_5-doped MgH_2 system. In this system, MgF_2 and Nb were observed by the reaction between MgH_2 and NbF_5. Thus, the chemical state of Nb was similar between AlH_3 and MgH_2 system. However, the existence of oxide species (Nb oxide, AlF_xO_y) could be one of the characteristics in the AlH_3 system. It is known that amorphous- or χ-Al_2O_3 film exists on the surface of AlH_3 particles. [13,14] Due to the lack of the standard Gibbs free energy of formation for amorphous- or χ-Al_2O_3, we considered the reaction with the most stable phase, α-Al_2O_3, as follows:

$$5\ Al_2O_3 + 6\ NbF_5 \rightarrow 3\ Nb_2O_5 + 10\ AlF_3$$

whose Gibbs free energy $\Delta G° = -1442.2$ kJ [11] is thermodynamically possible. Thus, NbF_5 could also react with surface Al_2O_3 film in the NbF_5-doped AlH_3 system. In order to clarify the detailed destabilization mechanism, *e.g.*, *in-situ* measurements on the reaction process between NbF_5 and surface Al_2O_3 film should be conducted. As the summary of XPS results, the formation of finely dispersed Nb species and/or AlF_3 could have the catalytic effect for hydrogen desorption of AlH_3. According to the previous

study, AlF_3-doped AlH_3 led to the decomposition of AlH_3 at room temperature [15], suggesting AlF_3 may have such catalytic effect.

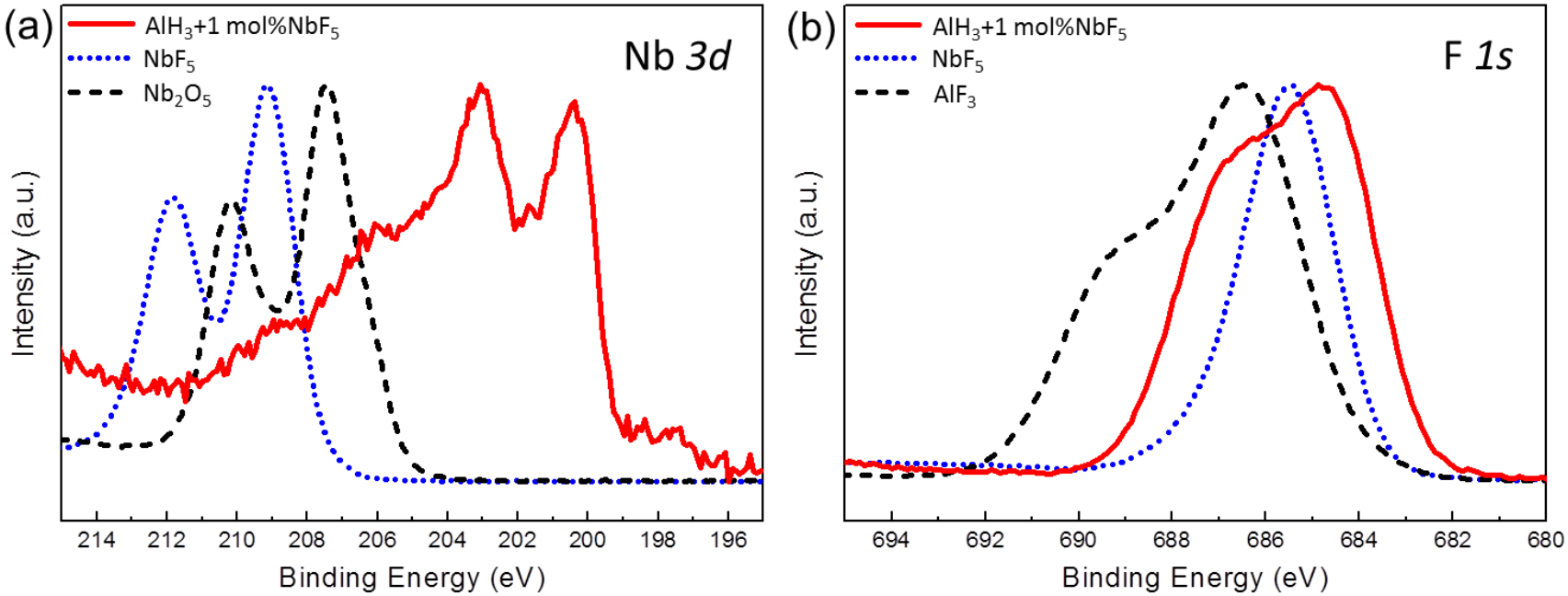

Fig.6-5 XPS spectra of (a) Nb *3d* and (b) F *1s* bands of 1 mol% NbF_5-doped AlH_3. The spectra of NbF_5, Nb_2O_5 and AlF_3 are also shown as references.

6.4 Summary

The addition of Nb species (Nb, Nb_2O_5, NbF_5) enhanced the hydrogen desorption properties of α-AlH_3. In particular, 1 mol% NbF_5-doped AlH_3 started to desorb hydrogen from 60 °C with a peak temperature at 122 °C. Compared with Nb- or Nb_2O_5-doped AlH_3, the fine distribution of dopant was observed in the NbF_5-doped AlH_3. The activation energy for hydrogen desorption was slightly decreased by doping NbF_5. From the XPS analysis, the NbF_5 reactions with AlH_3 and surface Al_2O_3 film were suggested. The improvement in the NbF_5-doped AlH_3 might be ascribed to the formation of finely distributed Nb and/or AlF_3.

Reference

1. F. M. Brower *et al., J. Am. Chem. Soc.* 98 (1976) 2450-2453
2. S. Orimo *et al., Appl. Phys. A* 83 (2006) 5-8
3. T. Ma, *et al., Int. J. Hydrogen Energy* 36 (2011) 12319-12323
4. J. W. Kim *et al., J. Power Sources* 178 (2008) 373-378
5. J. W. Kim *et al., Scr. Mater.* 62 (2010) 701-704
6. H. E. Kissinger, *Anal. Chem.* 29 (1957) 1702-1706
7. J. Graetz *et al., J. Phys. Chem.* B 109 (2005) 22181-22185
8. J. Graetz *et al., J. Alloys Comp.* 509S (2011) S517-S528
9. X. Wu *et al., Appl. Surf. Sci.* 201 (2002) 115-122
10. A. Limcharoen *et al., Procedia Engineering* 32 (2012) 1043-1049
11. D. D. Wagman *et al., J. Phys. Chem.* Ref. Data 11 (1982) Suppl. 2
12. J. Graetz, J. Reilly, G. Sandrock, J. Johnson, W. M. Zhou, J. Wegrzyn, Brookhaven National Laboratory Formal Report BNL-77336-2006 (2006)
13. S. Muto *et al., J. Appl. Phys.* 105 (2009) 123514
14. K. Ikeda *et al., Mater. Trans.* 52 (2011) 598-601
15. J. E. Fonneløp, *et al., J. Alloys Comp.* 509 (2011) 10-14

Chapter 7 General conclusion

Ammonia borane (NH_3BH_3) and Aluminum hydride (AlH_3) were selected from the DOE as high capacity hydrogen storage materials. However, each material has problems and cannot be used as it is. We conducted various experiments to improve the problem and five conclusions were obtained.

7.1 Synthesize of sodium-magnesium amidoborane

The synthesize of Na-Mg amidoborane (Na-Mg-$(NH_2BH_3)_n$, n= 3, 4) has been investigated in the Chapter 2 and 3 by using ball-milling method.

(1) Na-Mg amidoborane was synthesized under the conditions of $3NH_3BH_3 + MgH_2 +$ NaH and $3NH_3BH_3 + MgH_2 + NaNH_2$.

(2) In the case of the combination of $3NH_3BH_3$, MgH_2, $NaBH_4$, the reactivity of $NaBH_4$ and NH_3BH_3 was low and it was not possible to synthesis Na-Mg amidoborane

(3) In the combination of AB, MgH_2 and NaH, the $NaNH_2BH_3$ was synthesized in addition to Na-Mg amidoborane.

(4) A milling time of 12 hours is required for the sample to react sufficiently.

When $NaMg(NH_2BH_3)_3$ is compared with $Na_2Mg(NH_2BH_3)_4$, even in the composition in which $NaMg(NH_2BH_3)_3$ is formed, $Na_2Mg(NH_2BH_3)_4$ was formed as shown in the following reaction formula.

$$3NH_3BH_3+MgH_2+NaNH_2 \rightarrow 1/2Na_2Mg(NH_2BH_3)_4+NH_3BH_3+1/2MgH_2+NH_3+H_2$$

At a molar ratios of $NH_3BH_3 : MgH_2 : NaNH_2 = 4 : 1 : 2$, $Na_2Mg(NH_2BH_3)_4$ and $Na_2Mg(NH_2BH_3)_4 \cdot nNH_3$ were formed as in the following reaction formula.

$$4\ NH_3BH_3 + MgH_2 + 2\ NaNH_2 \rightarrow Na_2Mg(NH_2BH_3)_4 + 2\ NH_3 + 2\ H_2$$
$$\rightarrow (1-x)\ Na_2Mg(NH_2BH_3)_4 + x\ Na_2Mg(NH_2BH_3)_4 \cdot nNH_3 + 2\ H_2$$

7.2 Decomposition of sodium-magnesium amidoborane

The decomposition of Na-Mg amidoborane (Na-Mg-$(NH_2BH_3)_n$, n= 3, 4) has been investigated by XRD, TG-DTA, NMR and FTIR in the Chapter 3. Two types of Na-Mg

amidoborane ($NaMg(NH_2BH_3)_3$ and $Na_2Mg(NH_2BH_3)_4$) was synthesized under the same starting materials and milling condition.

(1) In the result of molar ratio 3 : 1 : 1, hydrogen was released in three exothermic reactions and one endothermic reaction. However, other experimental results showed that $Na_2Mg(NH_2BH_3)_4$ was synthesized. Thus, the endothermic dehydrogenation from Na-Mg amidoborane would originate from $Na_2Mg(NH_2BH_3)_4$

(2) In the result of molar ratio 4 : 1 : 2, phase, $Na_2Mg(NH_2BH_3)_4$ released hydrogen in one endothermic reaction. The products after the decomposition reaction were amorphous phase.

7.3 Re-hydrogenation of $Na_2Mg(NH_2BH_3)_4$

Normally, NH_3BH_3 is not capable of re-hydrogenation due to its hydrogen release mechanism. However, in the case of $Na_2Mg(NH_2BH_3)_4$, there is a possibility of re-hydrogenation since hydrogen was released endothermically. Since the change in enthalpy is as small as about -4 kJ/mol, pressurization experiments cannot be performed with a general pressure device. Therefore, the re-hydrogenation of $Na_2Mg(NH_2BH_3)_4$ has been investigated by using cubic-anvil-type high-pressure apparatus at Spring-8.

(1) The products produced after the high pressure experiment were different from the initial materials ($Na_2Mg(NH_2BH_3)_4$) and was not consistent with other expected compounds. Even after the decomposition of re-hydrogenation sample, the decomposition product was different from the results of Chapter 3. It became a new compound by re-hydrogenation.

(2) According to direct coupling MS measurement, this phase released hydrogen in several steps by raising the temperature.

7.4 Ammonia ab/desorption of $Na_2Mg(NH_2BH_3)_4$

The ammonia absorbed phase of $Na_2Mg(NH_2BH_3)_4$ was confirmed in Chapter 3. The ammonia ab/desorption of $Na_2Mg(NH_2BH_3)_4$ has been investigated.

(1) $Na_2Mg(NH_2BH_3)_4$ absorbed ammonia gas to form ammonia absorbed Na-Mg amidoborane ($Na_2Mg(NH_2BH_3)_4 \cdot nNH_3$) as a new solid phase. This phase further continued to absorb ammonia to form liquid phase.

(3) In the desorption profile of ammonia, the difference between the absorption amounts of 3 - 5 is probably due to the phase difference produced during absorption and desorption. There are two plateaus at absorption, so two phases could be created. On the other hand, since there is one plateaus at desorption, the ammonia absorption phase of the liquid changes into a single solid phase. Alternatively, there may be a problem with the PCI measurement temperature setting.

7.5 Doping effect of Nb species on hydrogen desorption properties of AlH_3

Hydrogen desorption properties of α-AlH_3 doped with Nb species (Nb, Nb_2O_5 and NbF_5) have been investigated in Chapter 6.

(1) All the Nb species showed the improvement of the desorption properties of AlH_3. Among them, 1 mol% NbF_5-doped AlH_3 showed the lowest desorption temperature from 60 °C. As a results of calculation by the Kissinger method, the apparent activation energy of hydrogen desorption of AlH_3 was slightly decreased with the dopant of NbF_5.

(2) The formation of NbH and Nb_2O_5 was observed after ball-milling. On the other hand, Nb- or F-containing phases were not observed in any diffraction patterns of the NbF_5-doped AlH_3. From the results of SEM-EDS, a fine distribution of the dopant was observed in the NbF_5 doped AlH_3 as compared to Nb- or Nb_2O_5-doped AlH_3.

(3) The improvement of desorption properties might be due to the finely dispersed Nb and/or AlF_3, which are formed by the reaction between NbF_5 and AlH_3.

As mentioned above, there was a possibility that AB could be re-hydrogenated as a result of my research. It has also opened new avenues for AB to use not only for hydrogen storage but also for ammonia transport. Finally, by confirming the state of Nb

doped to AlH_3, the mechanism of the additive effect can be understood and the effect can be predicted before the addition.

Acknowledgements

I still remember the day I entered LOAM. However my doctoral study is going to the end. During the past three and a half years, I have encountered all the difficulties. But with their help I was able to finally complete this dissertation. I will use acknowledgements to convey my gratitude.

First of all, I express my gratitude for Prof. Shigehito ISOBE who has always encouraged me in my Ph.D. course. During the past days he helped me a lot, both on my research and daily life. Every time when I was confused, his advices pointed out the right direction. Without his guidance and persistent help, this paper would not have been approved. In addition, when there was a problem in life, I was able to receive a scholarship by his recommendation.

At the same time, I would like to thank Prof. Naoyuki Hashimoto. Thanks for their every kind discussion that provided me with ideas, solutions and breakthroughs in my research. I learned so much from the conversation with them not only the knowledge, but also the way to think and handle with problems.

Also, I would like to thank Prof. Nakagawa. He has been so helpful on my research in more ways than one. Without His advice and comments, I would never have completed my Ph.D. course. I would like to take this opportunity to thank you again.

I would also like to thank my colleagues, Mr. K. OMORI, Y. SUZUKI, K. TOYOTA, T. OHKI, H. TANAKA, T. ISHIZUKA, Y. TANG, J. SHI, S. GOTO, M. KAMISAWA, N NOTO, K. SAKUMA, K. YAMAMOTO, Ms. C. Liu, N. KON and so on, for their cooperation on my work. Thanks to everyone, I was able to research happily.

Last but not least, I thank my family for their great support rearward. During the past years my wife always stood behind, bringing me happiness and soothing my sorrow. My parents always supported me silently and wholeheartedly.